L-Arginine Modulates T Cell Metabolism and Enhances Survival and Anti-tumor Activity

Journal Article

Author(s):
Geiger, Roger; Rieckmann, Jan C.; Wolf, Tobias; Basso, Camilla; Feng, Yuehan; Fuhrer, Tobias; Kogadeeva, Maria; Picotti, Paola; Meissner, Felix; Mann, Matthias; Zamboni, Nicola; Sallusto, Federica; Lanzavecchia, Antonio

Publication date:
2016-10-20

Permanent link:
https://doi.org/10.3929/ethz-b-000122202

Originally published in:
Cell 167(3), https://doi.org/10.1016/j.cell.2016.09.031

Article

Cell

L-Arginine Modulates T Cell Metabolism and Enhances Survival and Anti-tumor Activity

Graphical Abstract

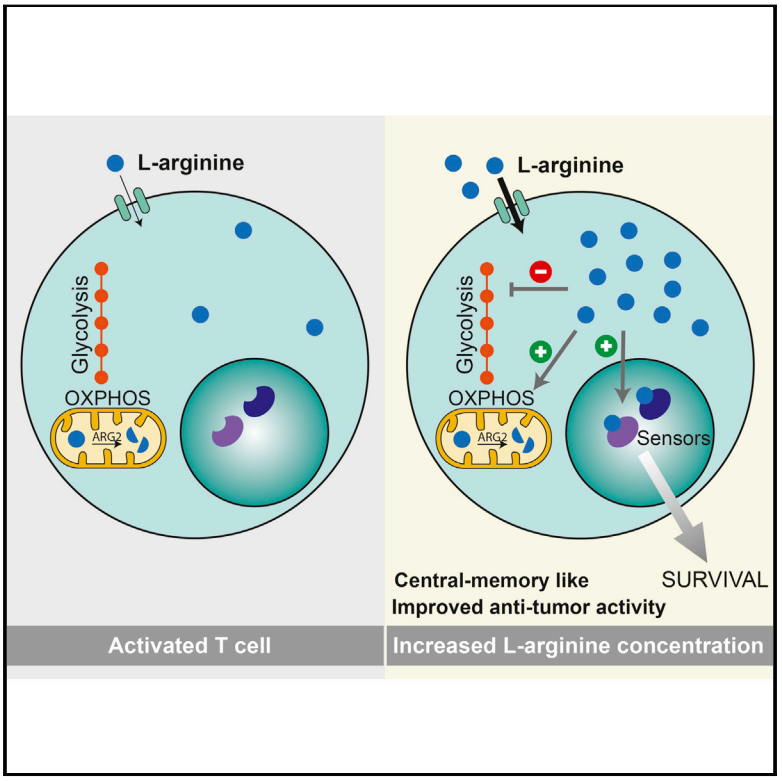

Authors

Roger Geiger, Jan C. Rieckmann, Tobias Wolf, ..., Nicola Zamboni, Federica Sallusto, Antonio Lanzavecchia

Correspondence

roger.geiger@irb.usi.ch (R.G.), lanzavecchia@irb.usi.ch (A.L.)

In Brief

Metabolomic and proteomic profiling unveil intracellular L-arginine as a crucial regulator of metabolic fitness, survival capacity, and anti-tumor activity of central memory T cells.

Highlights

- Dataset on dynamic metabolome/proteome profiles of activated human naive T cells
- Intracellular L-arginine levels regulate several metabolic pathways in T cells
- T cells with increased L-arginine display enhanced survival and anti-tumor activity
- LiP-MS identified proteins that are structurally modified by high L-arginine levels

Geiger et al., 2016, Cell *167*, 829–842
October 20, 2016
http://dx.doi.org/10.1016/j.cell.2016.09.031

CellPress

Article

Cell

L-Arginine Modulates T Cell Metabolism and Enhances Survival and Anti-tumor Activity

Roger Geiger,[1,2,*] Jan C. Rieckmann,[3] Tobias Wolf,[1,2] Camilla Basso,[1] Yuehan Feng,[4] Tobias Fuhrer,[5] Maria Kogadeeva,[5] Paola Picotti,[4] Felix Meissner,[3] Matthias Mann,[3] Nicola Zamboni,[5] Federica Sallusto,[1,6] and Antonio Lanzavecchia[1,2,7,*]

[1]Institute for Research in Biomedicine, Università della Svizzera italiana, Bellinzona 6500, Switzerland
[2]Institute of Microbiology, ETH Zurich, Zurich 8093, Switzerland
[3]Department of Proteomics and Signal Transduction, Max Planck Institute of Biochemistry, Martinsried 82152, Germany
[4]Institute of Biochemistry, ETH Zurich, Zurich 8093, Switzerland
[5]Institute of Molecular Systems Biology, ETH Zurich, Zurich 8093, Switzerland
[6]Center of Medical Immunology, Institute for Research in Biomedicine, Università della Svizzera italiana, Bellinzona 6500, Switzerland
[7]Lead Contact
*Correspondence: roger.geiger@irb.usi.ch (R.G.), lanzavecchia@irb.usi.ch (A.L.)
http://dx.doi.org/10.1016/j.cell.2016.09.031

SUMMARY

Metabolic activity is intimately linked to T cell fate and function. Using high-resolution mass spectrometry, we generated dynamic metabolome and proteome profiles of human primary naive T cells following activation. We discovered critical changes in the arginine metabolism that led to a drop in intracellular L-arginine concentration. Elevating L-arginine levels induced global metabolic changes including a shift from glycolysis to oxidative phosphorylation in activated T cells and promoted the generation of central memory-like cells endowed with higher survival capacity and, in a mouse model, anti-tumor activity. Proteome-wide probing of structural alterations, validated by the analysis of knockout T cell clones, identified three transcriptional regulators (BAZ1B, PSIP1, and TSN) that sensed L-arginine levels and promoted T cell survival. Thus, intracellular L-arginine concentrations directly impact the metabolic fitness and survival capacity of T cells that are crucial for anti-tumor responses.

INTRODUCTION

Upon antigenic stimulation, antigen-specific naive T cells proliferate extensively and acquire different types of effector functions. To support cell growth and proliferation, activated T cells adapt their metabolism to ensure the generation of sufficient biomass and energy (Fox et al., 2005). Unlike quiescent T cells, which require little nutrients and mostly use oxidative phosphorylation (OXPHOS) for their energy supply, activated T cells consume large amounts of glucose, amino acids, and fatty acids and adjust their metabolic pathways toward increased glycolytic and glutaminolytic activity (Blagih et al., 2015; Rolf et al., 2013; Sinclair et al., 2013; Wang et al., 2011).

At the end of the immune response, most T cells undergo apoptosis, while a few survive as memory T cells that confer long-term protection (Kaech and Cui, 2012; Sallusto et al., 2010). T cell survival is regulated by extrinsic and intrinsic factors. Prolonged or strong stimulation of the T cell receptor (TCR) of $CD4^+$ and $CD8^+$ T cells promotes "fitness" by enhancing survival and responsiveness to the homeostatic cytokines IL-7 and IL-15, which in turn sustain expression of anti-apoptotic proteins (Gett et al., 2003; Schluns and Lefrançois, 2003; Surh et al., 2006). Metabolic activity is also critical to determine T cell fate and memory formation (MacIver et al., 2013; Pearce et al., 2013; Wang and Green, 2012). For instance, triglyceride synthesis is central in IL-7-mediated survival of memory $CD8^+$ T cells (Cui et al., 2015), while increased mitochondrial capacity endows T cells with a bioenergetic advantage for survival and recall responses (van der Windt et al., 2012). Mitochondrial fatty acid oxidation is required for the generation of memory T cells (Pearce et al., 2009), while the mammalian target of rapamycin (mTOR), a central regulator of cell metabolism, has been shown to control T cell memory formation (Araki et al., 2009).

Metabolic fitness and T cell survival are particularly crucial in anti-tumor responses because nutrients are often scarce in the tumor microenvironment leading to T cell dysfunction (Chang et al., 2015; Ho et al., 2015), stress, and apoptosis (Alves et al., 2006; Maciver et al., 2008; Siska and Rathmell, 2015). Depletion of glucose may decrease production of interferon (IFN)-γ (Chang et al., 2013) and modulate the differentiation of regulatory T cells (De Rosa et al., 2015). In addition, degradation of L-arginine by myeloid-derived suppressor cells leads to reduced expression of the CD3ζ chain, resulting in impaired T cell responsiveness (Bronte and Zanovello, 2005; Rodriguez et al., 2007). L-arginine is a versatile amino acid that serves as a building block for protein synthesis and as a precursor for multiple metabolites, including, polyamines, and nitric oxide (NO) that have strong immunomodulatory properties (Grohmann and Bronte, 2010).

In this study, we took advantage of recent developments in mass spectrometry (Bensimon et al., 2012; Meissner and Mann, 2014; Zamboni et al., 2015) to obtain dynamic proteome and metabolome profiles of human primary naive T cells following activation and found several changes in metabolic pathways. In particular, we found that L-arginine controls

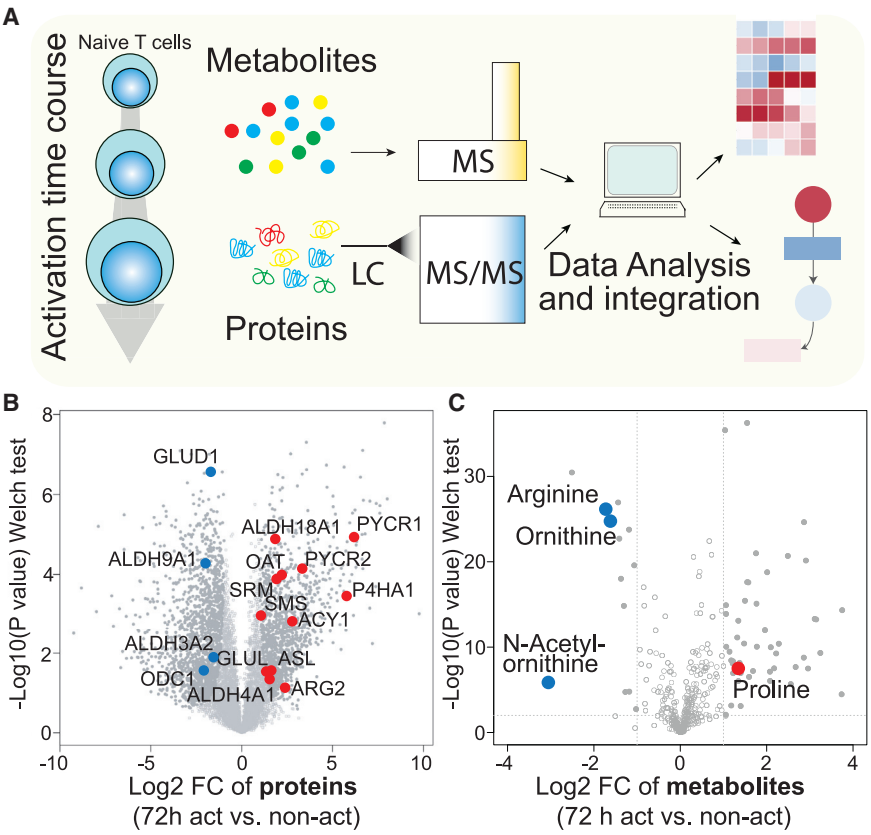

Figure 1. Metabolic and Proteomic Profiling Reveals Distinct Changes in L-Arginine Metabolism in Activated Human T Cells

(A) Schematic view of the experimental approach.

(B) Comparison of protein abundances between 72-hr-activated (CD3 + CD28 antibodies) and freshly isolated non-activated human naive $CD4^+$ T cells. Closed circles indicate proteins that changed significantly (FDR = 0.05, S_0 = 1). Colored dots are enzymes of the arginine and proline metabolism that changed significantly.

(C) Comparison of metabolite abundances in 72 hr-activated and freshly isolated non-activated human naive $CD4^+$ T cells. Closed circles indicate metabolites that changed significantly (|Log2 fc| > 1, p < 0.01). Colored dots are metabolites of the arginine and proline metabolism that changed significantly. Similar changes were observed when 72 hr-activated $CD4^+$ T cells were compared with naive $CD4^+$ T cells cultured overnight in the absence of TCR stimulation.

See also Figure S1 and Tables S1, S2, and S3.

glycolysis and mitochondrial activity and enhances T cell survival by interaction with transcriptional regulators. Moreover, L-arginine enhanced the generation of central memory-like T (Tcm) cells with enhanced anti-tumor activity in a mouse model.

RESULTS

Proteomic and Metabolomic Changes following Activation of Human Naive $CD4^+$ T Cells

To investigate the metabolic adaptations underlying T cell activation, we analyzed the cellular proteome and metabolome of human primary naive T cells using high-resolution mass spectrometry. Naive $CD45RA^+$ $CCR7^+$ $CD4^+$ T cells were sorted up to >98% purity from blood of healthy donors (Figure S1A) and either analyzed immediately after sorting or at different time points following activation with antibodies to CD3 and CD28. After cell lysis, proteins were digested and analyzed by liquid chromatography-coupled mass spectrometry (LC-MS) (Meissner and Mann, 2014; Nagaraj et al., 2011). In parallel, polar metabolites were extracted from cells at each time point and analyzed by non-targeted flow-injection metabolomics, a semi-quantitative method that allows rapid and deep profiling of metabolites, with the limitations that isobaric compounds cannot be discriminated and of possible in-source degradation (Fuhrer et al., 2011) (Figure 1A).

We identified a total of 9,718 proteins, quantified the abundance of 7,816 at each time point, and estimated their absolute copy numbers. Expression profiles of characteristic T cell proteins were in agreement with the literature and copy numbers of stable protein complexes had correct ratios (Figures S1B–S1G; Table S1). Non-targeted metabolomics led to the identification of 429 distinct ion species, which were putatively mapped to human metabolites (Table S2).

A comparative analysis of the proteome and metabolome of 72 hr activated and non-activated naive T cells identified 2,824 proteins whose relative expression changed significantly (Welch-test, false discovery rate [FDR] = 0.05, S_0 = 1), reflecting the fundamental morphological and functional alterations that T cells undergo upon activation (Figure 1B; Table S3). Upregulated proteins were enriched in enzymes of several metabolic pathways, including nucleotide synthesis, folate-mediated one-carbon metabolism, as well as arginine and proline metabolism. Out of 429 metabolites, 49 increased significantly (Log2 fold change [fc] > 1; p < 0.01), but only 14 were less abundant in activated T cells, of which three, arginine, ornithine, and N-acetylornithine, belonged to the same metabolic pathway (Figure 1C). Collectively, these data provide a comprehensive resource on the dynamics occurring in the proteome and metabolome of activated human primary naive $CD4^+$ T cells.

Intracellular L-Arginine Is Rapidly Metabolized in Activated T Cells

Based on the data obtained, we inspected the changes in the arginine metabolism more closely. The decrease in intracellular arginine occurred abruptly between 24 and 48 hr after T cell activation (Figure 2A). This finding was surprising in view of the high concentration of L-arginine in the medium (1 mM) and of the high uptake rate of ^{3}H-L-arginine in activated T cells, which exceeded

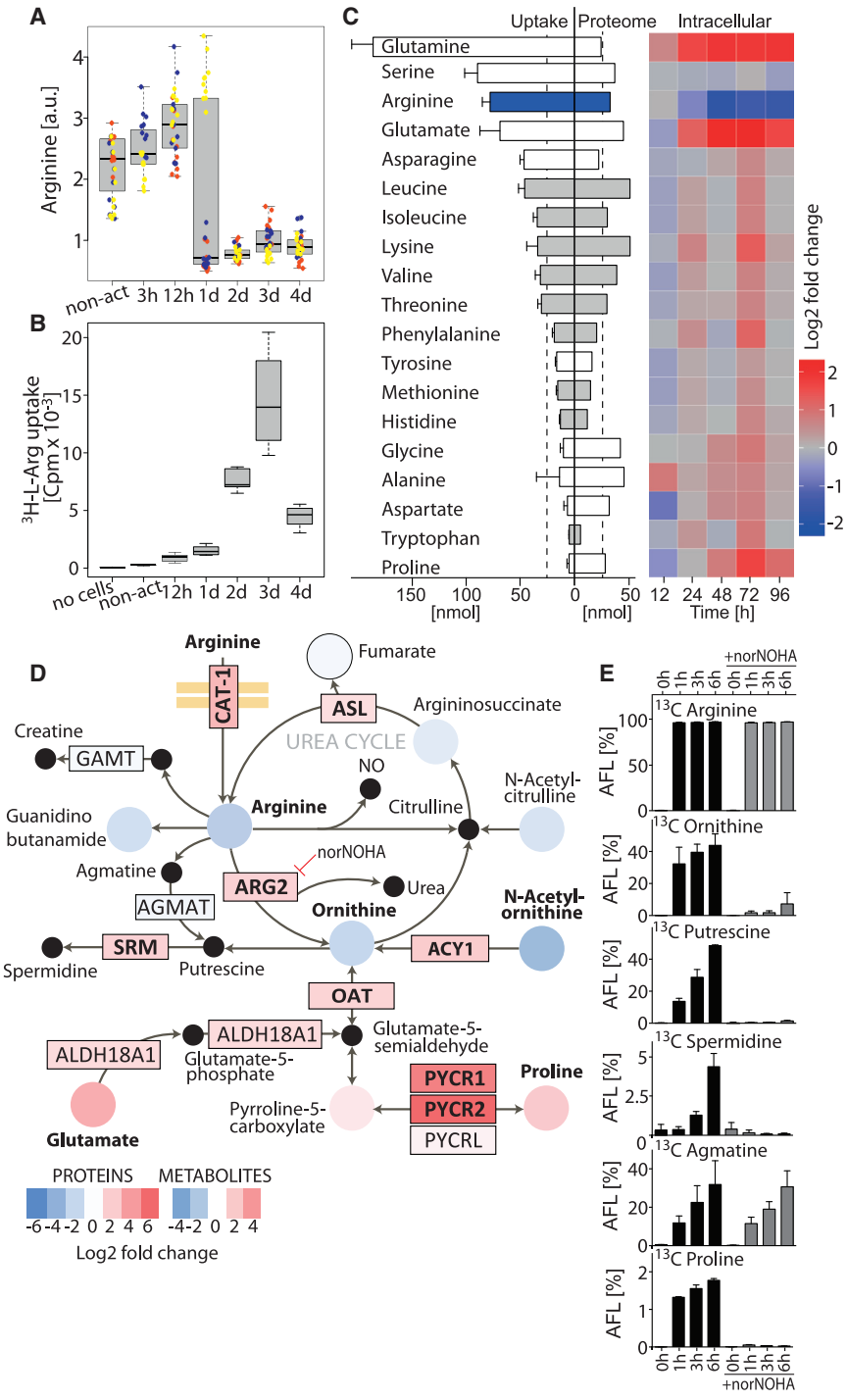

Figure 2. L-Arginine Is Rapidly Metabolized upon Activation

(A) Intracellular abundance of L-arginine in non-activated (non-act) and activated naive CD4$^+$ T cells (CD3 + CD28 antibodies). Boxplot, n = 30 from three donors, each in a different color.

(B) Kinetics of ^{3}H-L-arginine uptake during a 15-min pulse. Box plot, n = 5 from three donors.

(C) Uptake, proteome incorporation and intracellular abundance of the indicated amino acids. Barplot (left): 5 × 10^4 cells were activated for 4 days and consumption of amino acids from medium was analyzed. Essential amino acids are in gray; n = 4 from four donors, error bars represent SEM. Barplot (center): proteome incorporation of amino acids estimated from the copy numbers of each protein. Heat map (right): intracellular amino acid abundance relative to naive T cells over time as determined by mass spectrometry (MS) n = 30 from three donors. Leucine and isoleucine could not be distinguished as they have the same mass.

(D) Changes in the abundance of metabolites and proteins of the arginine and proline metabolism between non-activated and 72 hr-activated CD4$^+$ T cells. Log2 fold changes of proteins and metabolites are color-coded. Significant changes are in bold (FDR = 0.05, S_0 = 1 for proteins; and $p < 0.05$ [two-tailed unpaired Student's t test], $|\text{Log2 fc}| > 1$ for metabolites). Black dots are metabolites that were not detected by MS. Only enzymes that were detected by MS are shown.

(E) Metabolic tracing of L-arginine. Ninety-six hour-activated T cells were pulsed with $^{13}C_6$-L-arginine and the metabolic fate was analyzed by LC-MS/MS at different time points. AFL, apparent fractional labeling; n = 4 from two donors. ^{13}C Citrulline was not detected. Error bars represent SEM.

For (A) and (B), upper whisker = min(max(x), Q_3 + 1.5 * IQR) and lower whisker = max(min(x), Q_1 − 1.5 * IQR).

the requirement for protein synthesis by more than 2-fold (Figures 2C and 2B).

To gain insights into the metabolic fate of L-arginine, we analyzed the activation-induced changes in metabolites and proteins of the surrounding metabolic network (Figure 2D). While metabolites around the urea cycle were decreased, the arginine transporter cationic amino acid transporter 1 (CAT-1) and the enzymes arginase 2 (ARG2), ornithine aminotransferase (OAT), and spermidine synthase (SRM), which are required for the conversion of L-arginine into ornithine, L-proline, and spermidine, respectively, were upregulated. These findings suggest that L-arginine was rapidly converted into downstream metabolites. Indeed, ^{13}C-L-arginine tracing experiments showed an immediate and strong accumulation of ^{13}C in ornithine, putrescine, agmatine, and, to a lower extent, in spermidine and proline (Figure 2E). Addition of the arginase inhibitor norNOHA did not affect the conversion of L-arginine into agmatine, but markedly reduced the conversion into ornithine, putrescine, spermidine, and proline (Figure 2E). This indicated that in T cells L-arginine is mainly catabolized through arginase, likely through mitochondrial ARG2, because the cytosolic enzyme arginase 1 (ARG1) was not detected in T cells.

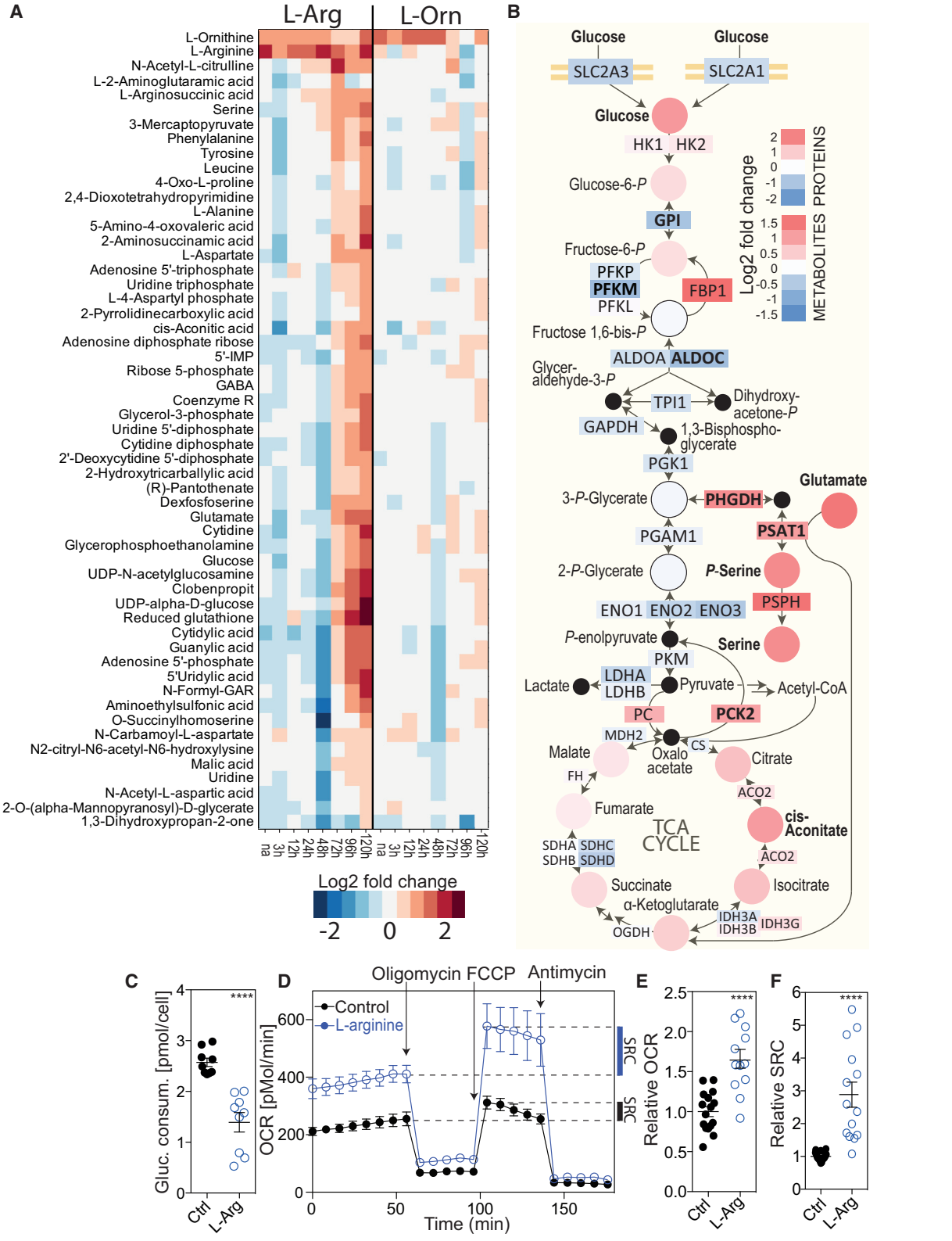

(legend on next page)

Collectively, these data show that L-arginine is avidly taken up by activated T cells in amounts exceeding the requirements for protein synthesis and can be rapidly converted by metabolic enzymes into downstream metabolites.

Elevated L-Arginine Levels Regulate Several Metabolic Pathways

Because activated T cells showed a drop in their intracellular arginine concentration—while all other amino acids either remained steady or increased—we assessed the consequences of increasing L-arginine availability on metabolism. We first performed a kinetic metabolome analysis of naive T cells activated in standard medium (containing 1 mM L-arginine) or in medium in which the concentration of L-arginine was increased 4-fold. Intracellular arginine and ornithine levels were increased 1.5- to 2.5-fold at all time points in T cells activated in L-arginine-supplemented medium as compared to controls (Figure 3A), while nitric oxide, which is generated from L-arginine by nitric oxide synthase (NOS), did not increase (Figure S2A). Notably, at late time points after activation (72–120 hr), several other metabolites, including intermediates of the urea cycle, nucleotides, sugar derivatives, and amino acids were increased (Figure 3A). In contrast, an increased availability of L-arginine's downstream metabolites L-ornithine or L-citrulline (added to the culture medium at the same concentration as L-arginine) only had minor effects on metabolism (Figures 3A and S2B). These findings suggest that L-arginine directly regulates several metabolic pathways in activated T cells.

A proteome analysis showed that the expression of 202 out of 7,243 proteins was significantly different in T cells activated in L-arginine-supplemented medium (Table S4, ANOVA, FDR = 0.005, $S_0 = 5$, $|\text{Log2 fc}| > 1$), indicating that T cells were reprogrammed under the influence of increased intracellular L-arginine levels. In particular, PC, PCK2, and FBP1, which promote gluconeogenesis, were increased, while glucose transporters and glycolytic enzymes were decreased (Figure 3B). Indeed, these T cells consumed less glucose (Figure 3C), indicating that the glycolytic flux was diminished by L-arginine supplementation. Moreover, the serine biosynthesis pathway that branches from glycolysis and several intermediates of the mitochondrial tricarboxylic acid (TCA) cycle were upregulated (Figure 3B). Consistent with the fact that the TCA cycle fuels OXPHOS, L-arginine supplementation increased oxygen consumption 1.7-fold and augmented the mitochondrial spare respiratory capacity (SRC) (Figures 3D–3F). Collectively, these data demonstrate that an increase in intracellular L-arginine levels skewed the metabolism in activated T cells from glycolysis toward mitochondrial OXPHOS.

L-Arginine Influences Human T Cell Proliferation, Differentiation, and Survival

Naive T cells start to divide after an initial period of growth that lasts 24–40 hr. Subsequently, they divide rapidly and differentiate into effector T cells that produce inflammatory cytokines, such as IFN-γ, and into memory T cells that survive through homeostatic mechanisms (Schluns and Lefrançois, 2003; Surh et al., 2006). We therefore asked whether elevated intracellular L-arginine concentrations affect the fate of activated T cells. Naive $CD4^+$ T cells activated in L-arginine-supplemented medium showed a slightly delayed onset of proliferation, but once proliferation started, doubling rates were comparable to controls (Figures S3A and S3B). The onset of proliferation was not affected by D-arginine or by addition of L-lysine (a competitive inhibitor of L-arginine uptake; Figure S3A) to L-arginine-supplemented cultures (Figure S3C). Importantly, T cells activated in L-arginine-supplemented medium secreted much less IFN-γ than T cells cultured in control medium (Figure 4A). However, when these cells were re-activated, they were able to secrete IFN-γ in comparable amounts (Figure 4B), indicating that T cells primed in the presence of high L-arginine concentrations retained the capacity to differentiate into Th1 effector cells upon secondary stimulation. Because low production of cytokines is characteristic of $CCR7^+$ lymph node-homing Tcm cells (Sallusto et al., 1999), we analyzed the expression of CCR7 on day 10 after activation and found a higher fraction of proliferating $CCR7^+$ T cells in L-arginine supplemented cultures than in control cultures (Figure 4C). Collectively, these data indicate that increased intracellular L-arginine levels limit T cell differentiation and maintain cells in a Tcm-like state.

To test whether L-arginine affects T cell survival, we activated human naive $CD4^+$ and $CD8^+$ T cells, expanded them in the presence of IL-2 or IL-15, and measured their viability upon cytokine withdrawal. Strikingly, L-arginine supplementation significantly increased the survival of activated $CD4^+$ and $CD8^+$ T cells when cultured in the absence of exogenous cytokines (Figures 4D and 4E). L-arginine was most effective when added during the first 48 hr following T cell activation (Figure 4F). Conversely, L-lysine or D-arginine, which both inhibit L-arginine uptake

Figure 3. L-Arginine Globally Influences Metabolism of Activated Human T Cells

(A) Human naive $CD4^+$ T cells were activated in control medium (Ctrl) or in medium supplemented with 3 mM L-arginine (L-Arg) or 3 mM L-ornithine (L-Orn) and harvested at different time points. The heat map shows the difference between the abundance of metabolites in T cells cultured in L-Arg or L-Orn-medium and controls. Shown are only metabolites with a Log2 fc > 1 and an adjusted p value of < 0.05; n = 12 from two donors.

(B) Differential analysis of the glycolytic pathway between naive $CD4^+$ T cells cultured in L-Arg medium or Ctrl medium, 96 hr after activation. Log2 fold changes of proteins and metabolites are color-coded. Proteins or metabolites whose abundance changed significantly are in bold (for proteins FDR = 0.005, $S_0 = 5$, $|\text{Log2 fc}| > 1$ and for metabolites $p < 0.05$ (Student's t test), $|\text{Log2 fc}| > 1$). 3-*P*-glycerate and 2-*P*-glycerate could not be distinguished as they have the same mass.

(C) Seventy-two hour-activated T cells were plated in fresh medium and glucose consumption was determined enzymatically after 24 hr; n = 9 from three donors. Error bars represent SEM.

(D) Seahorse experiment performed with activated (96 hr) T cells from one donor. Oligomycin was injected after 56 min, FCCP after 96 min, and antimycin (to inhibit the respiratory chain) after 136 min. Data are representative of five independent experiments with different donors; n = 4. Error bars represent SEM.

(E and F) Relative oxygen consumption rate (OCR) (E) and relative spare respiratory capacity (SRC) (F) of activated (96 hr) T cells; n = 12 from three donors. ****$p < 0.0001$ (Student's t test). Error bars represent SEM.

See also Figure S2 and Table S4.

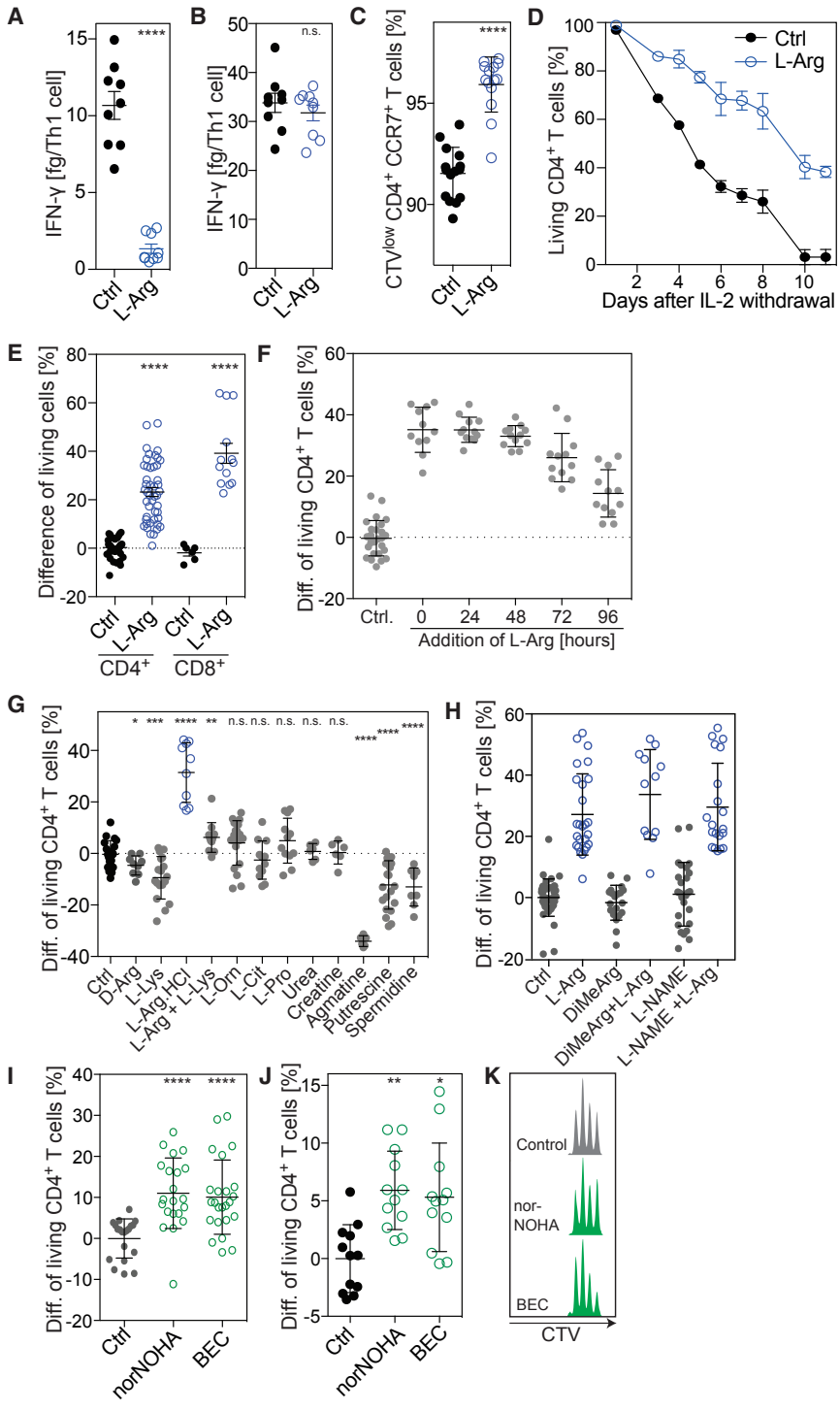

Figure 4. L-Arginine Limits Human T Cell Differentiation and Endows Cells with a High Survival Capacity In Vitro

(A and B) Human naive CD4$^+$ T cells were activated in L-Arg medium or Ctrl medium in the presence of 10 ng/mL IL-12. IFN-γ was quantified in culture supernatants after 5 days (A) or after re-activation for 5 hr with PMA/ionomycin (B); n = 9 from three donors.

(C) Naive CD4$^+$ T cells were labeled with CellTrace Violet (CTV) and activated in L-Arg medium or Ctrl medium. On day 10, proliferating CTV^{lo} T cells were stained with an antibody to CCR7 and analyzed by flow cytometry; n = 15 from three donors.

(D) Naive CD4$^+$ T cells were activated for 5 days in L-Arg or Ctrl medium in the presence of exogenous IL-2, washed extensively, and cultured in Ctrl medium in the absence of IL-2. Shown is the percentage of living T cells as determined by Annexin V staining at different time points after IL-2 withdrawal. One representative experiment out of three performed.

(E) Same experiment as in (D). Shown is the difference of living activated CD4$^+$ and CD8$^+$ T cells 5 days after withdrawal of IL-2; n = 46, from 16 donors (CD4$^+$ T cells); n = 13, from four donors (CD8$^+$ T cells).

(F) Difference of living activated CD4$^+$ T cells 5 days after IL-2 withdrawal. Naive CD4$^+$ T cells were activated and L-Arg (3 mM) was added to the culture medium at the indicated time points; n = 12 from four donors.

(G) Difference of living activated CD4$^+$ T cells 5 days after IL-2 withdrawal. Naive CD4$^+$ T cells were activated in Ctrl medium or medium supplemented with the indicated metabolites (3 mM, except for spermidine 0.1 mM). Ctrl, n = 21; D-Arg, n = 9; L-lysine, n = 18; L-Arg-HCl, n = 10; L-Arg + L-Lys, n = 12; L-Orn, n = 20; L-Cit, L-Pro, n = 12; urea, creatine, agmatine, n = 6; putrescine, n = 18; spermidine, n = 8, from at least three donors.

(H) Difference of living activated CD4$^+$ T cells 5 days after IL-2 withdrawal. Naive CD4$^+$ T cells were activated in the presence or absence of nitric oxide synthase inhibitors dimethylarginine (DiMeArg) or L-NG-nitroarginine methyl ester (L-NAME), both used at 1 mM. Ctrl and L-Arg, n = 26; DiMeArg and L-NAME, n = 16; DiMeArg + L-Arg and L-NAME + L-Arg, n = 12, from at least three donors.

(I) Difference of living activated CD4$^+$ T cells 5 days after IL-2 withdrawal. Naive CD4$^+$ T cells were activated in absence (Ctrl) or presence of the arginase inhibitors N$^{\omega}$-Hydroxy-nor-L-arginine (norNOHA, 300 μM) or S-(2-boronoethyl)-L-cysteine (BEC, 300 μM); n = 21, from seven donors.

(J) Same as in (I) but cultures were performed in medium containing 150 μM L-arginine.

(K) Effect of norNOHA and BEC on proliferation of CTV-labeled naive T cells measured 72 hr after activation. *p < 0.05, **p < 0.01, ***p < 0.001, ****p < 0.0001 (Student's t test).

(A–J) Error bars represent SEM throughout.

See also Figures S3 and S4.

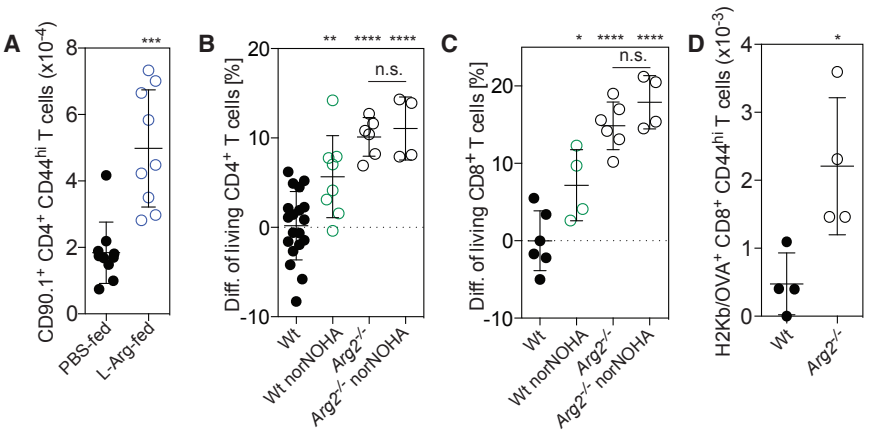

Figure 5. Increased Intracellular L-Arginine Levels Endow Mouse T Cells with a High Survival Capacity In Vitro and In Vivo

(A) BALB/c CD90.1$^+$ CD4$^+$ TCR transgenic T cells specific for the influenza $HA_{110–119}$ peptide were adoptively transferred into CD90.2$^+$ host mice that were then immunized subcutaneously (s.c.) with $HA_{110–119}$ in complete Freund's adjuvant (CFA). Mice were fed with L-arginine-HCl (1.5 mg/g body weight) or PBS, administrated daily starting 1 day before immunization. Fifteen days later, the amount of CD44^{hi} CD90.1$^+$ CD4$^+$ TCR transgenic T cells in draining lymph nodes was measured by fluorescence-activated cell sorting (FACS) analysis; n = 9 from two independent experiments.

(B and C) In vitro T cell survival experiment with C57BL/6 wild-type (WT) or *Arg2*$^{-/-}$ T cells. Naive CD62L^{hi} CD44^{lo} CD4$^+$ T cells and CD8$^+$ T cells were activated for 4 days in L-Arg or Ctrl medium in the absence or presence of the arginase inhibitor norNOHA (500 μM). On day 2 exogenous IL-2 was added to the cultures, on day 4 cells were washed extensively and cultured in medium without IL-2. Shown is the difference in the percentage of living CD4$^+$ (B) and CD8$^+$ (C) T cells relative to WT T cells as determined by Annexin V staining 2 days after IL-2 withdrawal. WT, n = 6-19; WT norNOHA, n = 6–8; *Arg2*$^{-/-}$, n = 4–6; *Arg2*$^{-/-}$ norNOHA, n = 4.

(D) Equal numbers of CD45.1$^+$ WT and CD45.2$^+$ CD90.2$^+$ *Arg2*$^{-/-}$ naive CD8$^+$ T cells were transferred into CD45.2$^+$ CD90.1$^+$ host mice. Mice were immunized with the $OVA_{257–264}$ peptide in CFA. Fifteen days after immunization, the amount of $OVA_{257–264}$-specific CD44^{hi} CD8$^+$ T cells was measured in draining lymph nodes by flow cytometry using $OVA_{257–264}$/H-2Kb multimers; n = 4. One representative experiment out of two performed. *p < 0.05, **p < 0.01, ***p < 0.001, ****p < 0.0001 (Student's t test).

Error bars represent SEM throughout.

See also Figure S5.

(Figure S3C), decreased T cell survival significantly (Figure 4G), indicating that reduced availability of intracellular L-arginine negatively affects T cell survival. L-arginine's downstream metabolites ornithine, citrulline, proline, urea, and creatine, as well as nitric oxide, had no effect, while agmatine, putrescine, or spermidine decreased T cell survival (Figure 4G and 4H). L-arginine-HCl enhanced T cell survival to a similar extent than free base L-arginine, ruling out a possible influence of pH. The increased T cell survival induced by elevated intracellular L-arginine concentration was independent of mTOR signaling (Araki et al., 2009), based on the finding that L-arginine supplementation did not change phosphorylation levels of two targets of mTOR (p70 S6K1 and 4E-BP) and inhibition of mTOR by rapamycin, although enhancing T cell survival, affected metabolism in an entirely different way than L-arginine (Figures S4A–S4D).

To further support the notion that L-arginine regulates T cell survival, we inhibited arginase (that converts L-arginine into L-ornithine) with norNOHA or BEC, which increase intracellular L-arginine levels (Monticelli et al., 2016). Inhibition of arginase significantly increased the survival capacity of activated CD4$^+$ T cells, even in medium containing physiological levels of L-arginine (150 μM) (Figures 4I and 4J). Inhibition of arginase did not affect proliferation (Figure 4K), indicating that polyamines can be synthesized from other sources than L-arginine, i.e., from L-glutamate (Wang et al., 2011), a finding that is consistent with the experiments showing that polyamine synthesis only partially depends on L-arginine (Figure 2E).

Collectively, these data indicate that elevated intracellular L-arginine levels directly induced metabolic changes and longevity of human CD4$^+$ and CD8$^+$ T cells, independently of mTOR signaling or downstream metabolites.

L-Arginine Influences Mouse T Cell Survival In Vivo

To address the impact of changes in intracellular L-arginine levels in vivo, we performed experiments in mice. Naive TCR transgenic CD4$^+$ T cells specific for a hemagglutinin peptide ($HA_{110–119}$) were adoptively transferred into BALB/c mice that received daily supplements of L-arginine (1.5 mg/g body weight) or PBS as a control. This amount of arginine doubled the daily dietary intake present in chow. Mice were immunized with $HA_{110–119}$ in CFA and the amount of transgenic T cells in draining lymph nodes was measured 15 days later. Three times more CD44^{hi} CD4$^+$ TCR transgenic T cells were recovered in mice fed with L-arginine compared to control mice (Figure 5A). In control experiments, we found that 30 min after oral administration, L-arginine levels in the serum increased from ~160 μM to 700 μM (Figure S5A) and intracellular L-arginine levels of CD44^{hi}-activated T cells increased ~2-fold (Figure S5B).

We then analyzed CD4$^+$ and CD8$^+$ T cells from *Arg2*-deficient mice. When compared to wild-type T cells, *Arg2*$^{-/-}$ T cells showed 20% higher baseline intracellular L-arginine levels (Figure S5C) and when stimulated in vitro with antibodies to CD3 and CD28, they survived significantly longer than wild-type T cells after IL-2 withdrawal (Figures 5B and 5C). Moreover, activation in the presence of the arginase inhibitor norNOHA, while increasing the survival of wild-type T cells, did not affect survival of *Arg2*$^{-/-}$ T cells (Figures 5B and 5C), indicating that in mouse T cells L-arginine degradation occurred mainly through ARG2. Finally, equal numbers of congenically marked wild-type and *Arg2*$^{-/-}$ CD8$^+$ T cells were co-transferred into wild-type mice that were immunized with the ovalbumin-peptide SIINFEKL ($OVA_{257–264}$) in CFA. Fifteen days after immunization, the number of MHC-I H-2K^b haplotype (Kb)-restricted $OVA_{257–264}$-specific CD44^{hi} CD8$^+$ T cells was measured in lymph nodes by multimer

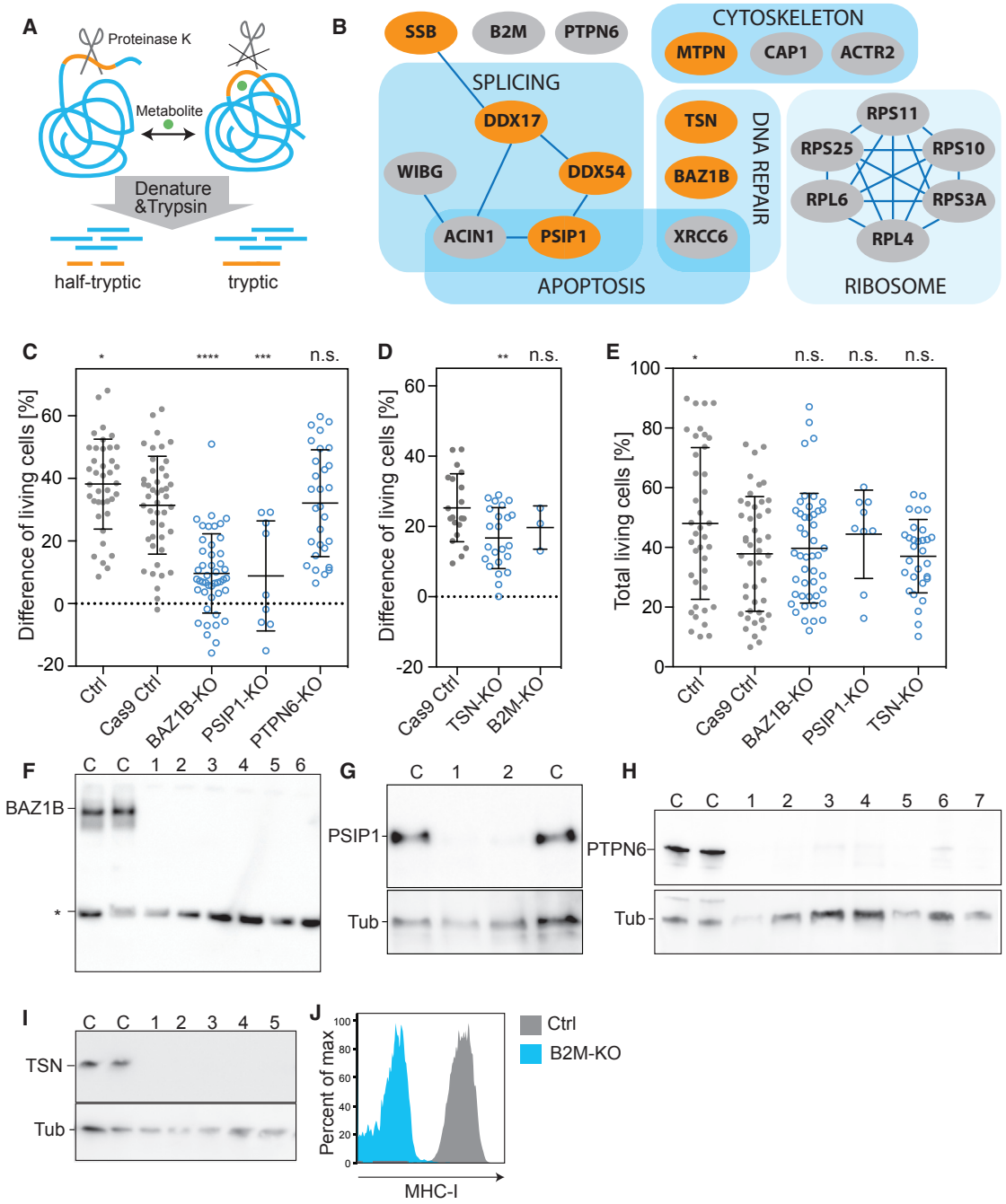

Figure 6. BAZ1B, PSIP1, and TSN Mediate the L-Arginine-Dependent Reprogramming of T Cells toward Increased Survival Capacity

(A) Scheme of the limited proteolysis workflow.

(B) Proteins that experience a structural change in response to 1 mM L-arginine but not to 1 mM D-arginine or L-ornithine. Transcriptional regulators are in orange, proteins are grouped according to their functions. Known interactions are indicated based on http://string-db.org/ and http://www.genemania.org/.

(C) Survival experiment with human $CD4^+$ T cell clones devoid of the indicated proteins. Control (Ctrl), n = 39; Cas9-transduced control (Cas9 Ctrl), n = 45; BAZ1B-KO, PSIP1-KO, and PTPN6-KO, n = 46, n = 9, and n = 29, respectively. Each T cell clone was analyzed in triplicate. Bars represent the mean ± SEM.

(D) Same as in (C). Cas9 Ctrl, n = 20; TSN-KO and B2M-KO, n = 23 and n = 3, respectively.

(E) Percentage of living cells after IL-2 withdrawal of T cells cultured in Ctrl medium. Ctrl, n = 39; Cas9 Ctrl, n = 45; BAZ1B-KO, PSIP1-KO, and TSN-KO, n = 46, n = 9, and n = 29, respectively.

(legend continued on next page)

staining. As shown in Figure 5D, OVA-specific *Arg2*$^{-/-}$ T cells were more numerous than OVA-specific wild-type T cells. Taken together, these findings provide evidence that intracellular L-arginine concentrations, which can be elevated by dietary supplementation, can increase the survival capacity of antigen-activated T cells in vivo.

Global Analysis of Structural Changes Identifies Putative L-Arginine Sensors

To elucidate the mechanism by which L-arginine promotes T cell survival, we first examined the list of differentially expressed proteins (Table S4) and found among the top hits Sirtuin-1, a histone deacetylase, which is known to increase the lifespan of different organisms (Tissenbaum and Guarente, 2001). However, a role for Sirtuin-1 was excluded based on the findings that human naive T cells activated in the presence of the Sirtuin-1 inhibitor Ex-527 and Sirtuin-1-deficient T cells generated using the CRISPR/Cas9 technology displayed a L-arginine-mediated increase in survival comparable to controls (Figure S6).

Given that L-arginine directly promotes T cell survival, we set out to identify putative protein interactors that may be modified by binding of L-arginine and initiate the pro-survival program. For this, we probed structural changes across the T cell proteome that occur in response to L-arginine following a recently developed workflow (Feng et al., 2014) (Figure 6A). T cells were homogenized and incubated in the absence or presence of 1 mM L-arginine, D-arginine, or L-ornithine. Subsequently, samples were subjected to limited proteolysis (LiP) with proteinase K, which preferentially cleaves flexible regions of a protein. After denaturation and trypsin digestion, peptide mixtures were analyzed by LC-MS. Because trypsin cleaves polypeptides specifically after lysine or arginine, cleavages after other amino acids were introduced by proteinase K, leading to half-tryptic peptides. Significant changes in the abundances of half-tryptic peptides (fc > 5, $p < 0.05$, > 2 peptides per protein) were used as readout for structural changes induced by the addition of metabolites.

Because L-arginine, but not D-arginine or L-ornithine, promoted T cell survival, we searched for proteins that were exclusively affected by L-arginine and were cleaved by proteinase K at identical sites in all samples from six donors. Out of 5,856 identified proteins, only 20 candidates fulfilled these stringent criteria (Figure 6B). These proteins differed widely in molecular weight and abundance (Table S5), excluding a bias toward large or abundant proteins. Most candidates were assigned to four functional groups: mRNA splicing, DNA repair, regulation of the cytoskeleton, and the ribosome, while seven were transcriptional regulators (in orange in Figure 6B). Thus, our global approach revealed several proteins with various functions that structurally respond to elevated intracellular L-arginine levels.

BAZ1B, PSIP1, and TSN Are Required for the L-Arginine-Mediated Effect on T Cell Survival

To test whether selected candidates identified through the structural analysis were involved in the L-arginine-mediated survival benefit, we generated gene knockout human T cell clones using the CRISPR/Cas9 system that were screened for loss of the corresponding protein by western blot or flow cytometry. Knockout of *PTPN6* (Shp-1) or *B2M* did not alter the effect of L-arginine on T cell survival (Figures 6C and 6D), while no viable clones were obtained after knockout of *XRCC6*, *ACIN1*, and *SSB* (not shown). Strikingly, knockout of the transcriptional regulators BAZ1B, PSIP1, and TSN significantly reduced L-arginine's beneficial effect on T cell survival (Figures 6C, 6D, and 6F–6J). Importantly, when cultured in control medium prior to the IL-2 withdrawal, T cell clones lacking these transcriptional regulators proliferated and survived like controls (Figure 6E), indicating that their viability was unaffected but they were unable to sense increased L-arginine levels and to induce the pro-survival program. Taken together, these data provide evidence that BAZ1B, PSIP1, and TSN interact with L-arginine and play a role in the reprograming of T cells toward increased survival capacity.

L-Arginine Improves Anti-tumor T Cell Response In Vivo

Because L-arginine increased the survival capacity of human and mouse T cells and favored the formation of Tcm-like cells that have been shown to be superior than effector memory T cells (Tem) in eradicating tumors in mouse models (Klebanoff et al., 2005), we reasoned that increased intracellular L-arginine levels might positively affect anti-tumor T cell responses in vivo. We stimulated naive TCR transgenic CD8$^+$ OT-I T cells specific for the OVA$_{257–264}$ peptide in control or L-arginine-supplemented medium for 4 days and measured their survival in vitro following IL-2 withdrawal and in vivo after adoptive transfer into lymphopenic *Cd3e*$^{-/-}$ mice. Consistent with our previous data, L-arginine endowed OT-I T cells with a higher survival capacity both in vitro and in vivo (Figures 7A and 7B). Moreover, these T cells maintained a Tcm-like state and secreted less IFN-γ than controls after in vitro priming but upon reactivation, they produced even more IFN-γ than controls (Figures 7C–7E). Remarkably, when adoptively transferred into wild-type mice bearing B16 melanoma tumors expressing the OVA antigen, L-arginine-treated OT-I T cells mounted a superior anti-tumor response, as measured by the reduction of tumor size and by the increased survival of mice (Figures 7F and 7G). Naive OT-I T cells primed in vivo by OVA + Alum immunization of tumor-bearing mice that were fed with L-arginine were also superior in mediating an anti-tumor response compared to OT-I T cells primed in mice fed with PBS (Figure 7H). Collectively, these data demonstrate that elevated L-arginine levels increased the survival capacity of CD8$^+$ T cells and their anti-tumor activity in vivo.

(F–I) Western blots or FACS analysis of T cell clones showing deletion of target proteins. C refers to Cas9 Ctrl clones. Unspecific bands are marked with asterisk. An antibody to tubulin (Tub) was used as a loading control. B2M-KO was verified by staining cells with an antibody against MHC-I. *$p < 0.05$, **$p < 0.01$, ***$p < 0.001$, ****$p < 0.0001$ (Student's t test).

(C–E) Error bars represent SEM throughout.

See also Figure S6 and Table S5.

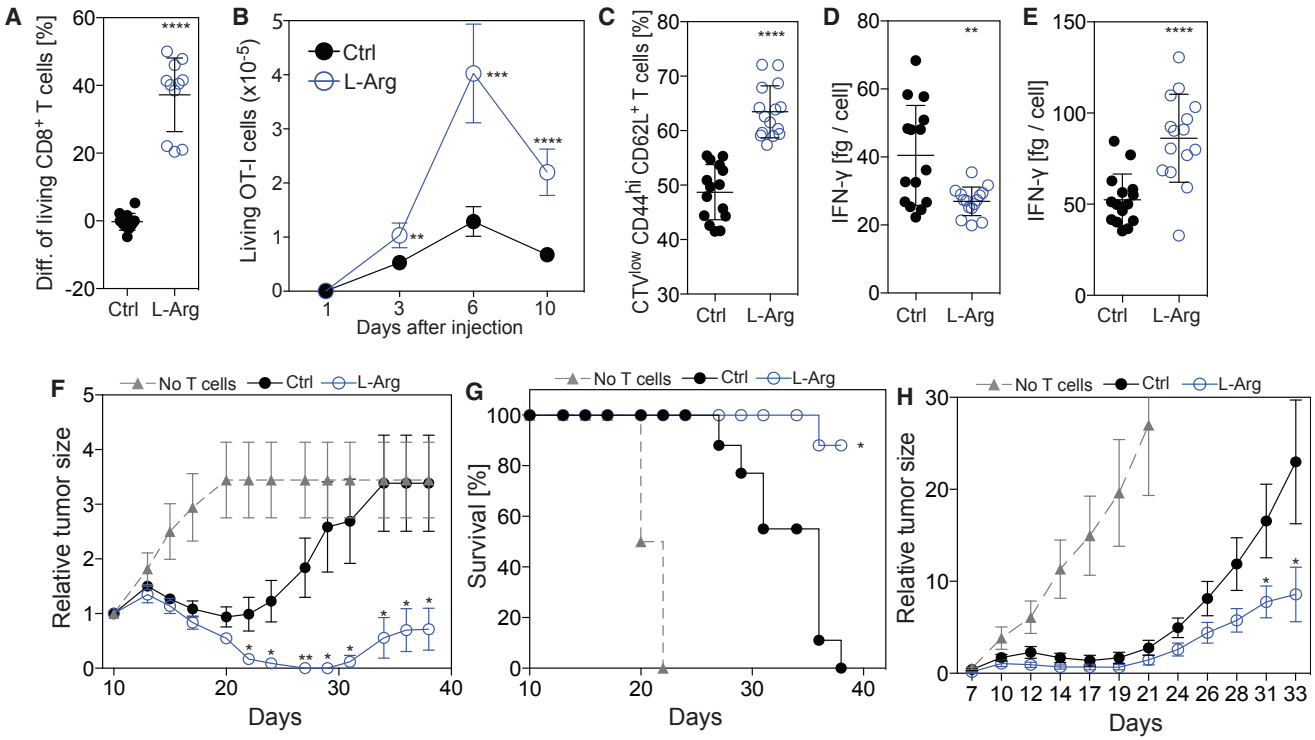

Figure 7. CD8⁺ T Cells with Increased L-Arginine Levels Display Improved Anti-tumor Activity In Vivo

(A) Survival of activated mouse CD8⁺ OT-I T cells (4 days) after IL-2 withdrawal. Data points represent the difference between the percentage of living T cells from cultures performed in L-Arg medium or Ctrl medium; n = 11.

(B) CD90.1⁺ CD45.1/2⁺ and CD90.1⁺ CD45.1⁺ naive CD8⁺ OT-I T cells were activated for 4 days in Ctrl medium or L-Arg medium, respectively. Equal numbers of the congenically marked activated OT-I cells were co-transferred into *Cd3e*$^{-/-}$ mouse and the number of living T cells was measured in pooled spleen and lymph nodes at the indicated time points; n = 3 at each time point.

(C) Naive CD8⁺ OT-I T cells were activated with CD3 + CD28 antibodies in L-Arg medium or Ctrl medium. Five days after activation, the percentage of Tcm-like cells (CD44^{hi}, CD62L⁺) was measured by flow cytometry; n = 15.

(D) Naive OT-I CD8⁺ T cells were activated in L-Arg medium or Ctrl medium and IFN-γ was quantified in culture supernatants after 5 days; n = 15.

(E) Same as in (D) but T cells were re-activated on day 5 day with PMA/Ionomycin; n = 15.

(F and G) B16.OVA melanoma cells were injected into C57BL/6 mice and tumors were allowed to grow for 10 days. Naive OT-I CD8⁺ T cells were activated in vitro in L-Arg medium or Ctrl medium and injected into tumor bearing mice. Tumor burden (F) and survival (G) were assessed over time. Data are representative of three independent experiments, each performed with seven to nine mice per group.

(H) B16.OVA melanoma cells were injected into C57BL/6 mice and tumors were allowed to grow for 6 days. At day 6, naive CD8⁺ OT-I T cells were transferred into tumor bearing mice and at day 7 mice were immunized with OVA peptide. Starting one day before the T cell transfer, PBS or L-arginine (1.5 mg/g body weight) was orally administered daily; n = 19 from three independent experiments. Bars represent the SEM. *p < 0.05, **p < 0.01, ***p < 0.001, ****p < 0.0001 (Student's t test). In (G), *p < 0.05 as determined by log-rank test comparison between curves.

Error bars represent SEM throughout.

DISCUSSION

Using proteomics, metabolomics, and functional approaches, we have shown that increased L-arginine levels can exert pleiotropic effects on T cell activation, differentiation, and function, ranging from increased bioenergetics and survival to in vivo anti-tumor activity.

We found that activated T cells heavily consume L-arginine and rapidly convert it into downstream metabolites, which lead to a marked decrease in intracellular levels after activation. Addition of exogenous L-arginine to the culture medium increased intracellular levels of free L-arginine and of several other metabolites and induced a metabolic switch from glycolysis to OXPHOS, thus counteracting the Warburg effect (Vander Heiden et al., 2009). While the mechanism by which L-arginine induces the broad metabolic changes remains elusive, a possible explanation for the switch toward OXPHOS is that increased L-arginine levels upregulate the serine biosynthesis pathway, which has been shown to fuel the TCA cycle and consequently OXPHOS (Possemato et al., 2011). Suggestive evidence for a link between L-arginine and the functionality of mitochondria has been provided by earlier observations; L-arginine improves mitochondrial function and reduces apoptosis of bronchial epithelial cells after injury induced by allergic airway inflammation (Mabalirajan et al., 2010) and had a beneficial effect for the treatment of patients with a mitochondrial disorder (Koga et al., 2010).

A striking finding is that a 2-fold increase in intracellular L-arginine concentrations induces human and mouse T cells to acquire

a Tcm-like phenotype with high expression of CCR7 and CD62L and a decreased production of IFN-γ. This may be a consequence of decreased glycolysis induced by L-arginine, as previous studies demonstrated that glycolytic activity supports IFN-γ mRNA translation (Chang et al., 2013). Although we observed a delayed onset of cell proliferation, L-arginine-treated T cells progressed through cell division in a way comparable to controls and readily proliferated and differentiated to effector cells upon secondary stimulation. Furthermore, inhibition of arginases in human T cells or deletion of ARG2 in mouse T cells did not affect cell proliferation, suggesting that the downstream fate of L-arginine is less important in T cells than the levels of free L-arginine. L-arginine may induce some of its pleiotropic effects through interfering with arginine methyltransferases, which can affect the functions of various proteins (Geoghegan et al., 2015).

Improved T cell survival is another striking effect induced by elevated intracellular L-arginine levels. Having excluded a role for L-arginine-derived nitric oxide and for the metabolic regulator Sirtuin-1 that has been shown to increase lifespan of lower eukaryotes (Tissenbaum and Guarente, 2001) and reduce glycolytic activity (Rodgers et al., 2005), which in T cells may enhance memory T cell formation and anti-tumor responses (Sukumar et al., 2013), we considered a direct effect of L-arginine on protein functions. Metabolite-protein interactions are more frequent than previously appreciated (Li et al., 2010), and in some cases, such interactions may have functional consequences. For instance, cholesterol binds to ~250 proteins (Hulce et al., 2013) and succinate, an intermediate of the TCA cycle, stabilizes HIF-1α in macrophages, leading to increased secretion of IL-1β (Tannahill et al., 2013). We took advantage of a novel method that allows proteome-wide probing of metabolite-protein interactions without modifying metabolites (Feng et al., 2014) and identified several proteins that changed their structure in the presence of L-arginine, which were likely sensors required to mediate the metabolic and functional response. We provide evidence that three nuclear proteins (BAZ1B, PSIP1, and TSN) were required in T cells for mediating L-arginine's effect on survival. BAZ1B is a transcriptional regulator containing a PHD domain that supposedly binds to methylated histones. PSIP1 is a transcriptional co-activator implicated in protection from apoptosis (Ganapathy et al., 2003). Interestingly, the structural changes induced by L-arginine affect the PHD domain of BAZ1B and the AT-hook DNA-binding domain of PSIP1, which may affect DNA binding and lead to the induction of the pro-survival program. Finally, TSN, a small DNA and RNA binding protein, has been implicated in DNA repair, regulation of mRNA expression, and RNAi (Jaendling and McFarlane, 2010) and can thus influence the cellular phenotype in various ways. The conclusion that these three proteins are involved in the pro-survival effect mediated by L-arginine is based on the analysis of several different knockout T cell clones. Yet, there was variability in the response to L-arginine, which may suggest compensatory mechanisms. This would be consistent with our finding that several independent proteins can sense L-arginine and contribute to the improved survival capacity. Future studies are needed to clarify the mechanism of how L-arginine affects the structure and functions of the identified sensors in vivo and how this translates into increased survival.

While in this study we addressed the response to elevated L-arginine levels, it is well established that T cells also sense L-arginine depletion, as it may occur in tumor microenvironments or when myeloid suppressor cells degrade L-arginine through ARG1 (Bronte and Zanovello, 2005). We have shown that moderately reduced uptake of L-arginine has a negative impact on T cell survival without affecting proliferation. However, when L-arginine was completely depleted from the culture medium, T cells no longer proliferated (data not shown and Rodriguez et al., 2007). Lack of L-arginine in T cells can be sensed by GCN2, leading to an amino acid starvation response (Rodriguez et al., 2007) and by SLC38A9, leading to inhibition of mTOR (Rebsamen et al., 2015; Wang et al., 2015), which in turn inhibits T cell growth and proliferation.

Our findings that T cells with increased L-arginine levels display improved anti-tumor activity may be due to a combination of phenotypic changes, including improved survival capacity, metabolic adaptations, and maintenance of a Tcm-like phenotype. L-arginine may also impact on other cell types in vivo, e.g., oral administration of L-arginine to healthy volunteers has been shown to enhance the numbers and activity of natural killer cells (Park et al., 1991). Future work is needed to address the exact mechanism by which L-arginine acts in vivo and favors memory T cell formation and anti-tumor responses.

Generally, metabolite levels can be influenced without genetic manipulations, offering the possibility for therapeutic applications. The beneficial effect of L-arginine on T cell survival and anti-tumor functionality may be exploited therapeutically, for instance to improve adoptive T cell therapies. Additionally, our dataset on the dynamics of the proteome and metabolome during the T cell response constitute a framework for future studies addressing the complex interplay between metabolism and cellular functions.

STAR★METHODS

Detailed methods are provided in the online version of this paper and include the following:

- KEY RESOURCES TABLE
- CONTACT FOR REAGENT AND RESOURCE SHARING
- EXPERIMENTAL MODEL AND SUBJECT DETAILS
  - Human Primary T Cells
  - Mice
- METHOD DETAILS
  - Isolation of Human T Cells
  - Cell Culture
  - Metabolomics
  - Metabolic Flux Experiments
  - Detection of Amino Acids and Polyamines by HILIC LC-MS/MS
  - Sample Preparation for Proteome MS Analysis
  - LC-MS/MS for Analysis of Proteome
  - Analysis of Proteomics Data
  - Limited Proteolysis and Mass Spectrometry
  - Quantitative Amino Acid Uptake and Calculation of Proteome Incorporation
  - ^{3}H-Arginine Uptake Assay

- OCR Measurements
- IL-2 Withdrawal Assay
- Cytokine Analysis
- Glucose Consumption Assay
- Analysis of Phosphorylation Levels of 4E-BP and S6K1
- CRISPR/Cas9-Mediated Gene Disruption
- Isolation and Culturing of Mouse $CD8^+$ T Cells
- Adoptive T Cell Transfers and Survival Experiments
- Tumor Experiments: In Vitro Activation of T Cells
- Tumor Experiments: In Vivo Priming of T Cells
- Experiments with *Arg2*$^{-/-}$ Mouse T Cells
- Mouse Experiments with Dietary L-Arginine

● QUANTIFICATION AND STATISTICAL ANALYSIS
- Proteome Data
- Enrichment Analysis

● DATA AND SOFTWARE AVAILABILITY

SUPPLEMENTAL INFORMATION

Supplemental Information includes six figures and six tables and can be found with this article online at http://dx.doi.org/10.1016/j.cell.2016.09.031.

AUTHOR CONTRIBUTIONS

R.G. conceived the project, designed and performed experiments, analyzed the data, and wrote the manuscript. T.W. designed and performed experiments and analyzed the data. J.R., R.G., and F.M. performed the proteomic experiments and analyzed the data. T.F., M.K., and N.Z. designed and performed metabolome and flux experiments and analyzed data. C.B. designed and performed mouse experiments. Y.F. and P.P. designed and performed limited proteolysis experiments. A.L., F.S., M.M., and N.Z. supervised the work and edited the manuscript.

ACKNOWLEDGMENTS

We thank Walter Reith, Isabelle Dunand-Sauthier, and Adria-Arnau Marti Lindez for providing the *Arg2*$^{-/-}$ mice, David Jarrossay for cell sorting, Luana Perlini for help with mouse experiments, Peter Mirtschink and Wilhelm Krek for providing access to the Seahorse analyzer, and members of the A.L., F.S., N.Z., and M.M. laboratories for discussions. This work was supported in part by the Swiss Vaccine Research Institute, the Swiss National Science Foundation (grant 149475 to A.L.), and the European Research Council (grant 323183 PREDICT to F.S.). R.G. was supported by a grant from the Swiss SystemsX.ch initiative, evaluated by the Swiss National Science Foundation. A.L. is supported by the Helmut Horten Foundation.

Received: February 3, 2016
Revised: March 18, 2016
Accepted: September 19, 2016
Published: October 13, 2016

REFERENCES

Alves, N.L., Derks, I.A., Berk, E., Spijker, R., van Lier, R.A., and Eldering, E. (2006). The Noxa/Mcl-1 axis regulates susceptibility to apoptosis under glucose limitation in dividing T cells. Immunity *24*, 703–716.

Araki, K., Turner, A.P., Shaffer, V.O., Gangappa, S., Keller, S.A., Bachmann, M.F., Larsen, C.P., and Ahmed, R. (2009). mTOR regulates memory CD8 T-cell differentiation. Nature *460*, 108–112.

Bellone, M., Cantarella, D., Castiglioni, P., Crosti, M.C., Ronchetti, A., Moro, M., Garancini, M.P., Casorati, G., and Dellabona, P. (2000). Relevance of the tumor antigen in the validation of three vaccination strategies for melanoma. J. Immunol. *165*, 2651–2656.

Bensimon, A., Heck, A.J., and Aebersold, R. (2012). Mass spectrometry-based proteomics and network biology. Annu. Rev. Biochem. *81*, 379–405.

Blagih, J., Coulombe, F., Vincent, E.E., Dupuy, F., Galicia-Vázquez, G., Yurchenko, E., Raissi, T.C., van der Windt, G.J., Viollet, B., Pearce, E.L., et al. (2015). The energy sensor AMPK regulates T cell metabolic adaptation and effector responses in vivo. Immunity *42*, 41–54.

Bronte, V., and Zanovello, P. (2005). Regulation of immune responses by L-arginine metabolism. Nat. Rev. Immunol. *5*, 641–654.

Carr, E.L., Kelman, A., Wu, G.S., Gopaul, R., Senkevitch, E., Aghvanyan, A., Turay, A.M., and Frauwirth, K.A. (2010). Glutamine uptake and metabolism are coordinately regulated by ERK/MAPK during T lymphocyte activation. J. Immunol. *185*, 1037–1044.

Chang, C.H., Curtis, J.D., Maggi, L.B., Jr., Faubert, B., Villarino, A.V., O'Sullivan, D., Huang, S.C., van der Windt, G.J., Blagih, J., Qiu, J., et al. (2013). Posttranscriptional control of T cell effector function by aerobic glycolysis. Cell *153*, 1239–1251.

Chang, C.H., Qiu, J., O'Sullivan, D., Buck, M.D., Noguchi, T., Curtis, J.D., Chen, Q., Gindin, M., Gubin, M.M., van der Windt, G.J., et al. (2015). Metabolic competition in the tumor microenvironment is a driver of cancer progression. Cell *162*, 1229–1241.

Cox, J., and Mann, M. (2008). MaxQuant enables high peptide identification rates, individualized p.p.b.-range mass accuracies and proteome-wide protein quantification. Nat. Biotechnol. *26*, 1367–1372.

Cox, J., and Mann, M. (2012). 1D and 2D annotation enrichment: a statistical method integrating quantitative proteomics with complementary high-throughput data. BMC Bioinformatics *13* (*Suppl 16*), S12.

Cox, J., Neuhauser, N., Michalski, A., Scheltema, R.A., Olsen, J.V., and Mann, M. (2011). Andromeda: a peptide search engine integrated into the MaxQuant environment. J. Proteome Res. *10*, 1794–1805.

Cui, G., Staron, M.M., Gray, S.M., Ho, P.C., Amezquita, R.A., Wu, J., and Kaech, S.M. (2015). IL-7-induced glycerol transport and TAG synthesis promotes memory CD8+ T cell longevity. Cell *161*, 750–761.

De Rosa, V., Galgani, M., Porcellini, A., Colamatteo, A., Santopaolo, M., Zuchegna, C., Romano, A., De Simone, S., Procaccini, C., La Rocca, C., et al. (2015). Glycolysis controls the induction of human regulatory T cells by modulating the expression of FOXP3 exon 2 splicing variants. Nat. Immunol. *16*, 1174–1184.

Feng, Y., De Franceschi, G., Kahraman, A., Soste, M., Melnik, A., Boersema, P.J., de Laureto, P.P., Nikolaev, Y., Oliveira, A.P., and Picotti, P. (2014). Global analysis of protein structural changes in complex proteomes. Nat. Biotechnol. *32*, 1036–1044.

Fox, C.J., Hammerman, P.S., and Thompson, C.B. (2005). Fuel feeds function: energy metabolism and the T-cell response. Nat. Rev. Immunol. *5*, 844–852.

Fuhrer, T., Heer, D., Begemann, B., and Zamboni, N. (2011). High-throughput, accurate mass metabolome profiling of cellular extracts by flow injection-time-of-flight mass spectrometry. Anal. Chem. *83*, 7074–7080.

Ganapathy, V., Daniels, T., and Casiano, C.A. (2003). LEDGF/p75: a novel nuclear autoantigen at the crossroads of cell survival and apoptosis. Autoimmun. Rev. *2*, 290–297.

Geoghegan, V., Guo, A., Trudgian, D., Thomas, B., and Acuto, O. (2015). Comprehensive identification of arginine methylation in primary T cells reveals regulatory roles in cell signalling. Nat. Commun. *6*, 6758.

Gett, A.V., Sallusto, F., Lanzavecchia, A., and Geginat, J. (2003). T cell fitness determined by signal strength. Nat. Immunol. *4*, 355–360.

Grohmann, U., and Bronte, V. (2010). Control of immune response by amino acid metabolism. Immunol. Rev. *236*, 243–264.

Ho, P.C., Bihuniak, J.D., Macintyre, A.N., Staron, M., Liu, X., Amezquita, R., Tsui, Y.C., Cui, G., Micevic, G., Perales, J.C., et al. (2015). Phosphoenolpyruvate is a metabolic checkpoint of anti-tumor T cell responses. Cell *162*, 1217–1228.

Hornburg, D., Drepper, C., Butter, F., Meissner, F., Sendtner, M., and Mann, M. (2014). Deep proteomic evaluation of primary and cell line motoneuron disease

models delineates major differences in neuronal characteristics. Mol. Cell. Proteomics *13*, 3410–3420.

Hubner, N.C., Ren, S., and Mann, M. (2008). Peptide separation with immobilized pI strips is an attractive alternative to in-gel protein digestion for proteome analysis. Proteomics *8*, 4862–4872.

Hubner, N.C., Bird, A.W., Cox, J., Splettstoesser, B., Bandilla, P., Poser, I., Hyman, A., and Mann, M. (2010). Quantitative proteomics combined with BAC TransgeneOmics reveals in vivo protein interactions. J. Cell Biol. *189*, 739–754.

Hulce, J.J., Cognetta, A.B., Niphakis, M.J., Tully, S.E., and Cravatt, B.F. (2013). Proteome-wide mapping of cholesterol-interacting proteins in mammalian cells. Nat. Methods *10*, 259–264.

Jaendling, A., and McFarlane, R.J. (2010). Biological roles of translin and translin-associated factor-X: RNA metabolism comes to the fore. Biochem. J. *429*, 225–234.

Kaech, S.M., and Cui, W. (2012). Transcriptional control of effector and memory CD8+ T cell differentiation. Nat. Rev. Immunol. *12*, 749–761.

Kirberg, J., Baron, A., Jakob, S., Rolink, A., Karjalainen, K., and von Boehmer, H. (1994). Thymic selection of CD8+ single positive cells with a class II major histocompatibility complex-restricted receptor. J. Exp. Med. *180*, 25–34.

Klebanoff, C.A., Gattinoni, L., Torabi-Parizi, P., Kerstann, K., Cardones, A.R., Finkelstein, S.E., Palmer, D.C., Antony, P.A., Hwang, S.T., Rosenberg, S.A., et al. (2005). Central memory self/tumor-reactive CD8+ T cells confer superior antitumor immunity compared with effector memory T cells. Proc. Natl. Acad. Sci. USA *102*, 9571–9576.

Koga, Y., Povalko, N., Nishioka, J., Katayama, K., Kakimoto, N., and Matsuishi, T. (2010). MELAS and L-arginine therapy: pathophysiology of stroke-like episodes. Ann. N Y Acad. Sci. *1201*, 104–110.

Lanzavecchia, A., and Scheidegger, D. (1987). The use of hybrid hybridomas to target human cytotoxic T lymphocytes. Eur. J. Immunol. *17*, 105–111.

Li, X., Gianoulis, T.A., Yip, K.Y., Gerstein, M., and Snyder, M. (2010). Extensive in vivo metabolite-protein interactions revealed by large-scale systematic analyses. Cell *143*, 639–650.

Link, H., Fuhrer, T., Gerosa, L., Zamboni, N., and Sauer, U. (2015). Real-time metabolome profiling of the metabolic switch between starvation and growth. Nat. Methods *12*, 1091–1097.

Luber, C.A., Cox, J., Lauterbach, H., Fancke, B., Selbach, M., Tschopp, J., Akira, S., Wiegand, M., Hochrein, H., O'Keeffe, M., and Mann, M. (2010). Quantitative proteomics reveals subset-specific viral recognition in dendritic cells. Immunity *32*, 279–289.

Mabalirajan, U., Ahmad, T., Leishangthem, G.D., Dinda, A.K., Agrawal, A., and Ghosh, B. (2010). L-arginine reduces mitochondrial dysfunction and airway injury in murine allergic airway inflammation. Int. Immunopharmacol. *10*, 1514–1519.

Maciver, N.J., Jacobs, S.R., Wieman, H.L., Wofford, J.A., Coloff, J.L., and Rathmell, J.C. (2008). Glucose metabolism in lymphocytes is a regulated process with significant effects on immune cell function and survival. J. Leukoc. Biol. *84*, 949–957.

MacIver, N.J., Michalek, R.D., and Rathmell, J.C. (2013). Metabolic regulation of T lymphocytes. Annu. Rev. Immunol. *31*, 259–283.

Malissen, M., Gillet, A., Ardouin, L., Bouvier, G., Trucy, J., Ferrier, P., Vivier, E., and Malissen, B. (1995). Altered T cell development in mice with a targeted mutation of the CD3-epsilon gene. EMBO J. *14*, 4641–4653.

Meissner, F., and Mann, M. (2014). Quantitative shotgun proteomics: considerations for a high-quality workflow in immunology. Nat. Immunol. *15*, 112–117.

Messi, M., Giacchetto, I., Nagata, K., Lanzavecchia, A., Natoli, G., and Sallusto, F. (2003). Memory and flexibility of cytokine gene expression as separable properties of human T(H)1 and T(H)2 lymphocytes. Nat. Immunol. *4*, 78–86.

Michalski, A., Damoc, E., Hauschild, J.P., Lange, O., Wieghaus, A., Makarov, A., Nagaraj, N., Cox, J., Mann, M., and Horning, S. (2011). Mass spectrometry-based proteomics using Q Exactive, a high-performance benchtop quadrupole Orbitrap mass spectrometer. Molecular & cellular proteomics : MCP *10*, M111 011015.

Monticelli, L.A., Buck, M.D., Flamar, A.L., Saenz, S.A., Tait Wojno, E.D., Yudanin, N.A., Osborne, L.C., Hepworth, M.R., Tran, S.V., Rodewald, H.R., et al. (2016). Arginase 1 is an innate lymphoid-cell-intrinsic metabolic checkpoint controlling type 2 inflammation. Nat. Immunol. *17*, 656–665.

Nagaraj, N., Wisniewski, J.R., Geiger, T., Cox, J., Kircher, M., Kelso, J., Pääbo, S., and Mann, M. (2011). Deep proteome and transcriptome mapping of a human cancer cell line. Mol. Syst. Biol. *7*, 548.

Olsen, J.V., Macek, B., Lange, O., Makarov, A., Horning, S., and Mann, M. (2007). Higher-energy C-trap dissociation for peptide modification analysis. Nat. Methods *4*, 709–712.

Ori, A., Banterle, N., Iskar, M., Andrés-Pons, A., Escher, C., Khanh Bui, H., Sparks, L., Solis-Mezarino, V., Rinner, O., Bork, P., et al. (2013). Cell type-specific nuclear pores: a case in point for context-dependent stoichiometry of molecular machines. Mol. Syst. Biol. *9*, 648.

Park, K.G., Hayes, P.D., Garlick, P.J., Sewell, H., and Eremin, O. (1991). Stimulation of lymphocyte natural cytotoxicity by L-arginine. Lancet *337*, 645–646.

Pearce, E.L., Walsh, M.C., Cejas, P.J., Harms, G.M., Shen, H., Wang, L.S., Jones, R.G., and Choi, Y. (2009). Enhancing CD8 T-cell memory by modulating fatty acid metabolism. Nature *460*, 103–107.

Pearce, E.L., Poffenberger, M.C., Chang, C.H., and Jones, R.G. (2013). Fueling immunity: insights into metabolism and lymphocyte function. Science *342*, 1242454.

Possemato, R., Marks, K.M., Shaul, Y.D., Pacold, M.E., Kim, D., Birsoy, K., Sethumadhavan, S., Woo, H.K., Jang, H.G., Jha, A.K., et al. (2011). Functional genomics reveal that the serine synthesis pathway is essential in breast cancer. Nature *476*, 346–350.

Rappsilber, J., Mann, M., and Ishihama, Y. (2007). Protocol for micro-purification, enrichment, pre-fractionation and storage of peptides for proteomics using StageTips. Nat. Protoc. *2*, 1896–1906.

Rebsamen, M., Pochini, L., Stasyk, T., de Araújo, M.E., Galluccio, M., Kandasamy, R.K., Snijder, B., Fauster, A., Rudashevskaya, E.L., Bruckner, M., et al. (2015). SLC38A9 is a component of the lysosomal amino acid sensing machinery that controls mTORC1. Nature *519*, 477–481.

Rodgers, J.T., Lerin, C., Haas, W., Gygi, S.P., Spiegelman, B.M., and Puigserver, P. (2005). Nutrient control of glucose homeostasis through a complex of PGC-1alpha and SIRT1. Nature *434*, 113–118.

Rodriguez, P.C., Quiceno, D.G., and Ochoa, A.C. (2007). L-arginine availability regulates T-lymphocyte cell-cycle progression. Blood *109*, 1568–1573.

Rolf, J., Zarrouk, M., Finlay, D.K., Foretz, M., Viollet, B., and Cantrell, D.A. (2013). AMPKα1: a glucose sensor that controls CD8 T-cell memory. Eur. J. Immunol. *43*, 889–896.

Sallusto, F., Lenig, D., Förster, R., Lipp, M., and Lanzavecchia, A. (1999). Two subsets of memory T lymphocytes with distinct homing potentials and effector functions. Nature *401*, 708–712.

Sallusto, F., Lanzavecchia, A., Araki, K., and Ahmed, R. (2010). From vaccines to memory and back. Immunity *33*, 451–463.

Sanjana, N.E., Shalem, O., and Zhang, F. (2014). Improved vectors and genome-wide libraries for CRISPR screening. Nat. Methods *11*, 783–784.

Scheltema, R.A., and Mann, M. (2012). SprayQc: a real-time LC-MS/MS quality monitoring system to maximize uptime using off the shelf components. J. Proteome Res. *11*, 3458–3466.

Schluns, K.S., and Lefrançois, L. (2003). Cytokine control of memory T-cell development and survival. Nat. Rev. Immunol. *3*, 269–279.

Shiow, L.R., Rosen, D.B., Brdicková, N., Xu, Y., An, J., Lanier, L.L., Cyster, J.G., and Matloubian, M. (2006). CD69 acts downstream of interferon-alpha/beta to inhibit S1P1 and lymphocyte egress from lymphoid organs. Nature *440*, 540–544.

Sinclair, L.V., Rolf, J., Emslie, E., Shi, Y.B., Taylor, P.M., and Cantrell, D.A. (2013). Control of amino-acid transport by antigen receptors coordinates the

metabolic reprogramming essential for T cell differentiation. Nat. Immunol. *14*, 500–508.

Siska, P.J., and Rathmell, J.C. (2015). T cell metabolic fitness in antitumor immunity. Trends Immunol. *36*, 257–264.

Subramanian, A., Tamayo, P., Mootha, V.K., Mukherjee, S., Ebert, B.L., Gillette, M.A., Paulovich, A., Pomeroy, S.L., Golub, T.R., Lander, E.S., and Mesirov, J.P. (2005). Gene set enrichment analysis: a knowledge-based approach for interpreting genome-wide expression profiles. Proc. Natl. Acad. Sci. USA *102*, 15545–15550.

Sukumar, M., Liu, J., Ji, Y., Subramanian, M., Crompton, J.G., Yu, Z., Roychoudhuri, R., Palmer, D.C., Muranski, P., Karoly, E.D., et al. (2013). Inhibiting glycolytic metabolism enhances CD8+ T cell memory and antitumor function. J. Clin. Invest. *123*, 4479–4488.

Surh, C.D., Boyman, O., Purton, J.F., and Sprent, J. (2006). Homeostasis of memory T cells. Immunol. Rev. *211*, 154–163.

Tannahill, G.M., Curtis, A.M., Adamik, J., Palsson-McDermott, E.M., McGettrick, A.F., Goel, G., Frezza, C., Bernard, N.J., Kelly, B., Foley, N.H., et al. (2013). Succinate is an inflammatory signal that induces IL-1β through HIF-1α. Nature *496*, 238–242.

Tissenbaum, H.A., and Guarente, L. (2001). Increased dosage of a sir-2 gene extends lifespan in Caenorhabditis elegans. Nature *410*, 227–230.

Tusher, V.G., Tibshirani, R., and Chu, G. (2001). Significance analysis of microarrays applied to the ionizing radiation response. Proc. Natl. Acad. Sci. USA *98*, 5116–5121.

van der Windt, G.J., Everts, B., Chang, C.H., Curtis, J.D., Freitas, T.C., Amiel, E., Pearce, E.J., and Pearce, E.L. (2012). Mitochondrial respiratory capacity is a critical regulator of CD8+ T cell memory development. Immunity *36*, 68–78.

Vander Heiden, M.G., Cantley, L.C., and Thompson, C.B. (2009). Understanding the Warburg effect: the metabolic requirements of cell proliferation. Science *324*, 1029–1033.

Wang, R., and Green, D.R. (2012). Metabolic checkpoints in activated T cells. Nat. Immunol. *13*, 907–915.

Wang, R., Dillon, C.P., Shi, L.Z., Milasta, S., Carter, R., Finkelstein, D., McCormick, L.L., Fitzgerald, P., Chi, H., Munger, J., and Green, D.R. (2011). The transcription factor Myc controls metabolic reprogramming upon T lymphocyte activation. Immunity *35*, 871–882.

Wang, S., Tsun, Z.Y., Wolfson, R.L., Shen, K., Wyant, G.A., Plovanich, M.E., Yuan, E.D., Jones, T.D., Chantranupong, L., Comb, W., et al. (2015). Metabolism. Lysosomal amino acid transporter SLC38A9 signals arginine sufficiency to mTORC1. Science *347*, 188–194.

Wiśniewski, J.R., Ostasiewicz, P., Duś, K., Zielińska, D.F., Gnad, F., and Mann, M. (2012). Extensive quantitative remodeling of the proteome between normal colon tissue and adenocarcinoma. Mol. Syst. Biol. *8*, 611.

Zamboni, N., Saghatelian, A., and Patti, G.J. (2015). Defining the metabolome: size, flux, and regulation. Mol. Cell *58*, 699–706.

STAR★METHODS

KEY RESOURCES TABLE

REAGENT or RESOURCE	SOURCE	IDENTIFIER
Antibodies		
Human CD4-APC (clone 13B8.2)	Beckman Coulter	Cat#IM2468; RRID: AB_130781
Human CD45RA-PE (clone ALB11)	Beckman Coulter	Cat#IM1834U
Human CCR7-BV421 (clone G043H7)	BioLegend	Cat#353208; RRID: AB_11203894
Human CCR7 (clone 15053)	R&D Systems	Cat#MAB197
Human CD25-FITC (clone B1.49.9)	Beckman Coulter	Cat#IM0478U; RRID: AB_130985
Human CD8-FITC (clone B9.11)	Beckman Coulter	Cat#A07756; RRID: AB_1575981
Human CD3 (clone TR66)	In house	Lanzavecchia and Scheidegger, 1987
Human CD28 (clone CD28.2)	BD Biosciences	Cat#555725; RRID: AB_396068
Human BAZ1B (WSTF) polyclonal	Abcam	Cat#AB50850; RRID: AB_870595
Human PSIP1 (LEDGF/p75) polyclonal	Bethyl laboratories	Cat#A300-848A
Human TSN polyclonal	Atlas antibodies/Sigma	Cat#HPA059561
Human PTPN6 (SH-PTP1, SHP-1) polyclonal	Santa Cruz	Cat#sc-287; RRID: AB_2173829
Human MHC-I (HLA-ABC) FITC (clone W6/32)	eBiosciences	Cat#11-9983-42
Human p70 S6 Kinase	Cell Signaling	Cat#9202; RRID: AB_331676
Human Phospho-p70 S6 Kinase (Thr389)	Cell Signaling	Cat#9205; RRID: AB_330944
Human 4E-BP1	Cell Signaling	Cat#9644; RRID: AB_2097841
Human Phospho-4EBP1 (Thr37/46)	Cell Signaling	Cat#2855; RRID: AB_560835
Anti-mouse CD4, Pacific Orange (clone RM4-5)	Invitrogen	Cat#MCD0430
Anti-mouse CD8a, Pacific Blue (clone 53-6.7)	Biolegend	Cat#100725; RRID: AB_493425
Anti-mouse/human CD44, APC/Cy7 (clone IM7)	Biolegend	Cat#103028; RRID: AB_830785
Anti-mouse/human CD44, FITC (clone IM7)	Biolegend	Cat#103022; RRID: AB_493685
Anti-mouse/human CD44, APC (clone IM7)	Biolegend	Cat#103012; RRID: AB_312963
Anti-mouse CD62L, PE/Cy7 (clone MEL-14)	Biolegend	Cat#104418; RRID: AB_313103
Anti-mouse 90.1, APC/Cy7 (clone OX-7)	Biolegend	Cat#202520; RRID: AB_2303153
LEAF purified anti-mouse CD3ε (clone 145-2C11)	Biolegend	Cat#100331; RRID: AB_1877073
Purified hamster anti-mouse CD28 (clone37.51)	BD Biosciences	Cat#553295; RRID: AB_394764
Chemicals, Peptides, and Recombinant Proteins		
L-arginine	Sigma	Cat#A5006
L-arginine monohydrochloride	Sigma	Cat#A4599
D-arginine	Sigma	Cat#A2646
L-Arginine-13C6 hydrochloride	Sigma	Cat#643440
L-[2,3,4-^{3}H]-arginine-monohydrochloride	Perkin Elmer	Cat#NET1123001MC
Annexin-V-FITC	Biolegend	Cat#640906
Cell-Tak	BD Biosciences	Cat#354240
Oligomycin	Sigma	Cat#75351
Carbonyl cyanide-*4*-(trifluoromethoxy) phenylhydrazone (FCCP)	Sigma	Cat#C2920
Antimycin	Sigma	Cat#A8674
Recombinant human interleukin-2	BD Biosciences	Cat#554603
Recombinant human interleukin-12	Biolegend	Cat#573002
Human recombinant interleukin-2 (transfected J588L cell supernatant)	In house	N/A
FlowCytomix basic kit	eBioscience	Cat#BMS8420FF
Flow Cytomix human Th1/Th2/Th9/Th17/Th22 13plex	eBioscience	Cat#BMS817FF

(*Continued on next page*)

Continued		
REAGENT or RESOURCE	SOURCE	IDENTIFIER
Phorbol 12-myristate 13-acetate (PMA)	Sigma	Cat#P1585
Ionomycin	Sigma	Cat#I0634
Rapamycin	Sigma	Cat#R8781
Proteinase K	Sigma	Cat#P2308
Critical Commercial Assays		
Glucose (GO) Assay Kit	Sigma	Cat#GAGO20-1KT
Experimental Models: Cell Lines		
Human: primary T lymphocytes	This paper	N/A
Mouse: primary T lymphocytes	This paper	N/A
HEK293T/17	ATCC	Cat#CRL-11268
B16.OVA	Matteo Bellone	Bellone et al., 2000
Experimental Models: Organisms/Strains		
Mouse: C57BL/6: (C57BL/6JOlaHsd)	Harlan	Cat#57
Mouse: BALB/c: (BALB/cOlaHsd)	Harlan	Cat#162
Mouse: *Cd3e*$^{-/-}$ C57BL/6	Malissen et al., 1995	N/A
Mouse: OT-I: (C57BL/6-Tg(TcraTcrb)1100Mjb/J)	The Jackson Laboratory	Cat#JAX003831
Mouse: *Rag1*$^{-/-}$: (B6.129S7-*Rag1*^{tm1Mom}/J)	The Jackson Laboratory	Cat#JAX002216
Mouse: *Arg2*$^{-/-}$: C57BL/6 (*Arg2*^{tm1Weo}/J)	The Jackson Laboratory	Cat#JAX020286
Mouse: Hemagglutinin (HA) TCR-transgenic (6.5) BALB/c	Kirberg et al., 1994	N/A
Recombinant DNA		
lentiCRISPR v2	Addgene	Cat#52961
psPAX	Addgene	Cat#12260
pMD2.G	Addgene	Cat#12259
Sequence-Based Reagents		
Short guide RNAs, see Table S6	This paper	N/A
Software and Algorithms		
MaxQuant	Cox and Mann, 2008	http://www.coxdocs.org/doku.php?id=maxquant:start
Perseus	Cox and Mann, 2012	http://www.coxdocs.org/doku.php?id=perseus:start
Progenesis-QI Version 2.0	Nonlinear Dynamics, Waters	http://www.nonlinear.com/progenesis/qi/
Proteome Discoverer 1.4 (SEQUEST HT search engine)	Thermo Fisher	https://www.thermofisher.com/order/catalog/product/IQLAAEGABSFAKJMAUH
R environment for statistical computing	N/A	https://www.r-project.org/

CONTACT FOR REAGENT AND RESOURCE SHARING

Further information and requests for reagents may be directed to, and will be fulfilled by the corresponding author Antonio Lanzavecchia (lanzavecchia@irb.usi.ch).

EXPERIMENTAL MODEL AND SUBJECT DETAILS

Human Primary T Cells

Blood from healthy male or female donors was obtained from the Swiss Blood Donation Center of Basel and Lugano, and used in compliance with the Federal Office of Public Health (authorization no. A000197/2 to F.S).

Mice

Wild-type (WT) C57BL/6J and BALB/c mice were obtained from Harlan (Italy). *Cd3e*$^{-/-}$ C57BL/6 mice, which lack all T cells but exhibit organized lymphoid organ structures and normal B cell development, have been described previously (Malissen et al., 1995). OT-I

(JAX 003831) mice were bred and maintained on a *Rag1*$^{-/-}$ (JAX 002216) background. WT C57BL/6 mice with different CD45 and CD90 alleles were bred in our facility, and crossed with *Rag1*$^{-/-}$ OT-I transgenic mice, to perform adoptive transfer experiments. *Arg2*$^{-/-}$ C57BL/6 (JAX 020286) mice were kindly provided by W. Reith. Hemagglutinin (HA) TCR-transgenic (6.5) BALB/c mice (Kirberg et al., 1994) specific for peptide 111-119 from influenza HA were kindly provided by J. Kirberg and bred in our facility. All mice were bred and maintained under specific pathogen-free conditions. Animals were treated in accordance with guidelines of the Swiss Federal Veterinary Office and experiments were approved by the Dipartimento della Sanità e Socialità of Canton Ticino.

METHOD DETAILS

Isolation of Human T Cells

Peripheral blood mononuclear cells (PBMCs) were isolated by Ficoll gradient centrifugation. CD4$^+$ T cells were enriched with magnetic microbeads (Miltenyi Biotec). Naive CD4$^+$ T cells were sorted as CD4$^+$ CCR7$^+$ CD45RA$^+$ CD25$^-$ CD8$^-$ on a FACS Aria III cell sorter (BD Biosciences). For cell staining, the following antibodies were used: anti-CD4-APC (allophycocyanin), clone 13B8.2; anti-CD8-APC, clone B9.11; anti-CD8-FITC (fluorescein isothiocyanate), clone B9.11; anti-CD4-FITC, clone 13B8.2; anti-CD45RA-PE (phycoerythrin), clone alb11; anti-CD25-FITC, clone B1.49.9 (all from Beckman Coulter); anti-CCR7-Brilliant Violet 421, clone G043H7 (Biolegend).

Cell Culture

Cells were cultured in RPMI-1640 medium supplemented with 2mM glutamine, 1% (v/v) non-essential amino acids, 1% (v/v) sodium pyruvate, penicillin (50 U ml^{-1}), streptomycin (50 μg ml^{-1}; all from Invitrogen), and 5% (v/v) human serum (Swiss Blood Center). Human T cells were activated with plate bound anti-CD3 (5 μg/ ml, clone TR66) and anti-CD28 (1 μg/ml, clone CD28.2, BD Biosciences) for 48 hr. Then, cells were cultured in IL-2 containing media (500 U/ml).

Metabolomics

Naive CD4$^+$ T cells were either analyzed directly after isolation or at different time points after activation with CD3 and CD28 antibodies. Cells were washed twice in 96-well plates with 75 mM ammonium carbonate at pH 7.4 and snap frozen in liquid nitrogen. Metabolites were extracted three times with hot (> 70°C) 70% ethanol. Extracts were analyzed by flow injection – time of flight mass spectrometry on an Agilent 6550 QTOF instrument operated in the negative mode, as described previously (Fuhrer et al., 2011). Typically 5,000-12,000 ions with distinct mass-to-charge (m/z) ratio could be identified in each batch of samples. Ions were putatively annotated by matching their measured mass to that of the compounds listed by the KEGG database for *Homo sapiens*, allowing a tolerance of 0.001 Da. Only deprotonated ions (without adducts) were considered in the analysis. In case of multiple matching, such as in the case of structural isomers, all candidates were retained.

Metabolic Flux Experiments

Naive CD4$^+$ T cells were activated and 4 days later extensively washed and pulsed with L-arginine free RPMI medium containing 1 mM [U-^{13}C]-L-Arginine hydrochloride (Sigma). After increasing pulse-times, cells were washed and snap frozen in liquid nitrogen. Metabolites were extracted and analyzed by HILIC LC-MS/MS.

Detection of Amino Acids and Polyamines by HILIC LC-MS/MS

Supernatants from extraction were dried at 0.12 mbar to complete dryness in a rotational vacuum concentrator setup (Christ, Osterode am Harz, Germany) and dried metabolite extracts were stored at −80°C. Dry metabolite extracts were resuspended in 100 μl water and 5 μl were injected on an Agilent HILIC Plus RRHD column (100 × 2.1mm × 1.8 μm; Agilent, Santa Clara, CA, USA). A gradient of mobile phase A (10 mM ammonium formate and 0.1% formic acid) and mobile phase B (acetonitrile with 0.1% formic acid) was used as described previously (Link et al., 2015). Flow rate was held constant at 400 μl/min and metabolites were detected on a 5500 QTRAP triple quadrupole mass spectrometer in positive MRM scan mode (SCIEX, Framingham, MA, USA).

Sample Preparation for Proteome MS Analysis

Samples were processed as described by (Hornburg et al., 2014). In brief, cell pellets were washed with PBS and lysed in 4% SDS, 10 mM HEPES (pH 8), 10 mM DTT. Cell pellets were heat-treated at 95°C for 10 min and sonicated at 4°C for 15 min (level 5, Bioruptor, Diagenode). Alkylation was performed in the dark for 30 min by adding 55 mM iodoacetamide (IAA). Proteins were precipitated overnight with acetone at −20°C and resuspended the next day in 8 M Urea, 10 mM HEPES (pH 8). A two-step proteolytic digestion was performed. First, samples were digested at room temperature (RT) with LysC (1:50, w/w) for 3h. Then, they were diluted 1:5 with 50 mM ammoniumbicarbonate (pH 8) and digested with trypsin (1:50, w/w) at RT overnight. The resulting peptide mixtures were acidified and loaded on C18 StageTips (Rappsilber et al., 2007). Peptides were eluted with 80% acetonitrile (ACN), dried using a SpeedVac centrifuge (Eppendorf, Concentrator plus, 5305 000.304), and resuspended in 2% ACN, 0.1% trifluoroacetic acid (TFA), and 0.5% acetic acid. For deeper proteome analysis a peptide library was built. For this, peptides from naive and activated T cells were separated according to their isoelectric point on dried gel strips with an immobilized pH gradient (SERVA IPG BlueStrips, 3-10 / 11 cm) into 12 fractions as described by Hubner et al., 2008 (Hubner et al., 2008).

LC-MS/MS for Analysis of Proteome

Peptides were separated on an EASY-nLC 1000 HPLC system (Thermo Fisher Scientific, Odense) coupled online to a Q Exactive mass spectrometer via a nanoelectrospray source (Thermo Fisher Scientific)(Michalski et al., 2011). Peptides were loaded in buffer A (0.5% formic acid) on in house packed columns (75 μm inner diameter, 50 cm length, and 1.9 μm C18 particles from Dr. Maisch GmbH). Peptides were eluted with a non-linear 270 min gradient of 5%–60% buffer B (80% ACN, 0.5% formic acid) at a flow rate of 250 nl/min and a column temperature of 50°C. Operational parameters were real-time monitored by the SprayQC software (Scheltema and Mann, 2012). The Q Exactive was operated in a data dependent mode with a survey scan range of 300-1750 m/z and a resolution of 70'000 at m/z 200. Up to 5 most abundant isotope patterns with a charge $\geq$ 2 were isolated with a 2.2 Th wide isolation window and subjected to higher-energy C-trap dissociation (HCD) fragmentation at a normalized collision energy of 25 (Olsen et al., 2007). Fragmentation spectra were acquired with a resolution of 17,500 at m/z 200. Dynamic exclusion of sequenced peptides was set to 45 s to reduce the number of repeated sequences. Thresholds for the ion injection time and ion target values were set to 20 ms and 3E6 for the survey scans and 120 ms and 1E5 for the MS/MS scans, respectively. Data were acquired using the Xcalibur software (Thermo Scientific).

Analysis of Proteomics Data

MaxQuant software (version 1.3.10.18) was used to analyze MS raw files (Cox and Mann, 2008). MS/MS spectra were searched against the human Uniprot FASTA database (Version May 2013, 88'847 entries) and a common contaminants database (247 entries) by the Andromeda search engine (Cox et al., 2011). Cysteine carbamidomethylation was applied as fixed and N-terminal acetylation and methionine oxidation as variable modification. Enzyme specificity was set to trypsin with a maximum of 2 missed cleavages and a minimum peptide length of 7 amino acids. A false discovery rate (FDR) of 1% was required for peptides and proteins. Peptide identification was performed with an allowed initial precursor mass deviation of up to 7 ppm and an allowed fragment mass deviation of 20 ppm. Nonlinear retention time alignment of all measured samples was performed in MaxQuant. Peptide identifications were matched across different replicates within a time window of 1 min of the aligned retention times. A library for 'match between runs' in MaxQuant was built from additional single shot analysis at various time points as well as from OFF gel fractionated peptides of naive and memory CD4 T cells. Protein identification required at least 1 razor peptide. A minimum ratio count of 1 was required for valid quantification events via MaxQuant's Label Free Quantification algorithm (MaxLFQ)(Cox and Mann, 2008; Luber et al., 2010). Data were filtered for common contaminants and peptides only identified by side modification were excluded from further analysis. In addition, it was required to have a minimum of two valid quantifications values in at least one group of replicates. Copy numbers were estimated based on the protein mass of cells (Wiśniewski et al., 2012). We set the protein mass of a naive T cell to 25 pg and of an activated T cell to 75 pg.

Limited Proteolysis and Mass Spectrometry

Naive $CD4^+$ T cells were washed twice with PBS and homogenized on ice under non-denaturing conditions (20 mM HEPES, 150 mM KCl and 10 mM $MgCl_2$ [pH 7.5]) using a tissue grinder (Wheaton, Millville, NJ, NSA). Homogenates were further passed several times through a syringe (0.45x12mm) on ice. Next, cell debris was removed by centrifugation and protein concentration of supernatants was determined by BCA assay (BCA Protein Assay Kit, Thermo Scientific, Rockford, IL, USA). L-arginine, D-arginine or L-ornithine was added to homogenates to a final concentration of 1 nmol per μg total protein, and incubated for 5 min at room temperature. As a control, samples without added metabolites were processed in parallel. Then, proteinase K from *Tritirachium album* (Sigma) was added at an enzyme to substrate ratio of 1:100, followed by an incubation of 5 min at room temperature. The digestion was stopped by boiling the reaction mixture for 3 min. Proteins were denatured by adding 10% sodium deoxycholate (DOC) solution (1:1, v/v) to the reaction mixture, followed by a second boiling step of 3 min. Disulfide bridges were reduced with 5 mM Tris(2-carboxyethyl)phosphine hydrochloride (Thermo Scientific) at 37°C for 30 min and subsequently free cysteines were alkylated with 40 mM IAA at 25°C for 30 min in the dark. DOC concentration of the mixture was diluted to 1% with 0.1 M ammonium bicarbonate (AmBiC) prior to a stepwise protein digestion with LysC (1:100, w/w) for 4 hr at 37°C and trypsin (1:100, w/w) overnight at 37°C. The resulting peptide mixture was acidified to pH < 2, loaded onto Sep-Pak tC18 cartridges (Waters, Milford, MA, USA), desalted and eluted with 80% acetonitrile. Peptide samples were dried using a vacuum centrifuge and resuspended in 0.1% formic acid for analysis by mass spectrometry.

Peptides were separated using an online EASY-nLC 1000 HPLC system (Thermo Fisher Scientific) operated with a 50 cm long in house packed reversed-phase analytical column (Reprosil Pur C18 Aq, Dr. Maisch, 1.9 μm) (Reprosil Pur C18 Aq, Dr. Maisch, 1.9 μm) before being measured on a Q-Exactive Plus (QE+) mass spectrometer. A linear gradient from 5%–25% acetonitrile in 240 min at a flowrate of 300 nl/min was used to elute the peptides from the column. Precursor ion scans were measured at a resolution of 70,000 at 200 m/z and 20 MS/MS spectra were acquired after higher-energy collision induced dissociation (HCD) in the Orbitrap at a resolution of 17,500 at 200 m/z per scan. The ion count threshold was set at 1,00 to trigger MS/MS, with a dynamic exclusion of 25 s. Raw data were searched against the *H. sapiens* Uniprot database using SEQUEST embedded in the Proteome Discoverer software (both Thermo Fisher Scientific). Digestion enzyme was set to trypsin, allowing up to two missed cleavages, one non-tryptic terminus and no cleavages at KP (lysine-proline) and RP (arginine-proline) sites. Precursor and fragment mass tolerance was set at 10 ppm and 0.02 Da, respectively. Carbamidomethylation of cysteines (+57.021 Da) was set as static modification whereas oxidation

(+15.995 Da) of methionine was set as dynamic modification. False discovery rate (FDR) was estimated by the Percolator (embedded in Proteome Discoverer) and the filtering threshold was set to 1%.

Label-free quantitation was performed using the Progenesis-QI Software (Nonlinear Dynamics, Waters). Raw data files were imported directly into Progenesis for analysis. MS1 feature identification was achieved by importing the filtered search results (as described above) from Proteome Discoverer into Progenesis to map the corresponding peptides based on their m/z and retention times. Annotated peptides were then quantified using the areas under their extracted ion chromatograms. Pairwise comparisons were performed with the untreated (no metabolite added) sample as a reference and peptide fold changes were calculated using three biological replicates per condition where the statistical significance was assessed with a two-tailed heteroscedastic Student's t test. A fold change was considered significant with an absolute change > 5 and a corresponding p value < 0.05. Only proteins with two or more peptides changing significantly (according to the aforementioned criteria) were taken into consideration.

Quantitative Amino Acid Uptake and Calculation of Proteome Incorporation

150,000 freshly isolated naive $CD4^+$ T cells were activated with plate bound CD3 and CD28 antibodies and cultured in the same medium for four days. As a control, medium without cells was co-cultured. Then cell supernatants and control media were analyzed by quantitative amino acid analysis (MassTrak, Waters) at the Functional Genomic Center in Zurich. Amino acid uptake was calculated as the difference between control media and cell supernatants. At the time of the measurement, we counted on average 1 Mio cells. We then calculated how much of each amino acid is incorporated into the proteome of 850,000 cells based on the amino acid sequences and copy numbers of each protein. Average copy numbers from the time point 72 hr were used.

^{3}H-Arginine Uptake Assay

Arginine uptake was measured as previously described for glutamine uptake (Carr et al., 2010). Briefly, resting or activated T cells were resuspended at a concentration of $1.5x10^7$ cells/ml in serum-free RPMI 1640 lacking L-arginine. 50 μl 8% sucrose/20% perchloric acid were layered to the bottom of a 0.5 ml Eppendorf tube and 200 μl 1-bromododecane on top of it (middle layer), followed by 50 μl L-arginine-free medium containing 1.5 mCi L-[2,3,4-^{3}H]-arginine-monohydrochloride (Perkin Elmer). Then, 100 μl cell suspension was added to the top layer and cells were allowed to take up radiolabeled L-arginine for 15 min at room temperature. Cells were then spun through the bromododecane into the acid/sucrose. This stops the reaction and separates cells from unincorporated ^{3}H-L-arginine. The bottom layer containing the cells was carefully removed and analyzed by liquid scintillation. As controls cell-free media were used.

OCR Measurements

Measurements were performed using a Seahorse XF-24 extracellular flux analyzer (Seahorse Bioscience). Naive $CD4^+$ T cells were sorted and activated with plate-bound CD3 and CD28 antibodies in complete medium or medium supplemented with 3 mM L-arginine. Four days later (in the morning), cells were pooled, carefully count and plated (7×10^5 cells/well) in serum-free unbuffered RPMI-1640 medium (Sigma) onto Seahorse cell plates coated with Cell-Tak (BD Bioscience). The serum-free unbuffered medium was not supplemented with L-arginine. Oligomycin (1.4 μM, Sigma), Carbonyl cyanide-*4*-(trifluoromethoxy)phenylhydrazone (FCCP, 0.6 μM, Sigma) and antimycin (1.4 μM, Sigma) were injected.

IL-2 Withdrawal Assay

Naive CD4 T cells were activated with plate-bound CD3 and CD28 antibodies. 48 hr after activation IL-2 was added to culture media (500 U ml^{-1}). After a further 3 days of culturing, cells were washed, counted, and equal cell numbers were plated in medium devoid of IL-2. The withdrawal medium was no longer supplemented with e.g., L-arginine. Cell viability was assessed with annexin V.

Cytokine Analysis

10^5 naive T cells were stimulated with plate bound anti-CD3 (5μg/ml^{-1}) and anti-CD28 (1μg/ml^{-1}) in the presence of IL-12 (10 ng/ml, R&D Systems) to polarize cells toward a Th1 phenotype. After 48 hr, cells were transferred into U-bottom plates and IL-2 (10 ng/ml, R&D Systems) was added. Three days later, supernatants were collected and interferon-γ was quantified using FlowCytomix assays (eBioscience). Samples were analyzed on a BD LSR Fortessa FACS instrument and quantification was performed with the FlowCytomix Pro 3.0 software. For re-stimulation, cells were cultured for 5 hr in the presence of 0.2 μM phorbol 12-myristate 13-acetate (PMA) and 1 μg/ml ionomycin (both from Sigma).

Glucose Consumption Assay

The amount of glucose in media was determined using the Glucose (GO) Assay Kit from Sigma. Consumption was calculated as the difference between glucose content in reference medium (co-incubated medium without cells) and cell supernatants.

Analysis of Phosphorylation Levels of 4E-BP and S6K1

Naive $CD4^+$ T cells were activated with plate-bound antibodies to CD3 and CD28. Four days after activation, cells were lysed and analyzed by western blot with the following antibodies obtained from Cell Signaling Technology. Phospho-p70 S6K(Thr389) #9205; p70 S6 Kinase #9202; Phospho-4E-BP1 (Thr37/46) #2855; 4E-BP1 #9644. Rapamycin (Sigma) was used at 100 nM.

CRISPR/Cas9-Mediated Gene Disruption

Two to four short guide RNAs (sgRNAs) per gene (Table S6) were designed using the online tool provided by the Zhang laboratory (http://tools.genome-engineering.org). Oligonucleotide pairs with BsmBI-compatible overhangs were annealed and cloned into the lentiviral vector lentiCRISPR v2 (Addgene plasmid # 52961) (Sanjana et al., 2014). For virus production, HEK293T/17 cells were transfected with lentiCRISPR v2, psPAX2 (Addgene # 12260) and pMD2.G (Addgene plasmid # 12259) at a 8:4:1 ratio using polyethylenimine and cultured in Dulbecco's modified Eagle medium supplemented with 10% fetal bovine serum (FBS), 1% sodium pyruvate, 1% non-essential amino acids, 1% kanamycin, 50 units/ml penicilin/streptomycin and 50 μM β-mercaptoethanol. The medium was replaced 12 hr after transfection and after a further 48 hr virus was harvested from supernatant. Cell debris was removed by centrifugation (10 min at 2000 rpm followed) followed by ultra-centrifugation (2.5 hr at 24'000 rpm) through a sucrose cushion.

Freshly isolated naive $CD4^+$ T cells were lentivirally transduced and activated with plate-bound CD3 and CD28 antibodies. 48 hr after activation IL-2 was added to culture media (500 U/ml^{-1}). 6 days after activation, cells were cultured for 2 days in medium supplemented with 1 μg/ml puromycin to select for cells expressing the lentiCRISPR v2 vector. Subsequently, cells were cultured in normal medium followed by additional two days in medium containing puromycin for a second selection step. Then, single cell clones were generated by limiting dilution as described in (Messi et al., 2003).

To screen for clones with disrupted target genes, individual clones were lysed with sample buffer containing 80 mM Tris (pH 6.8), 10.5% glycerol, 2% SDS and 0.00004% Bromophenol blue. Lysate of 100'000 cells was separated by SDS-PAGE followed, blotted onto PVDF membranes and analyzed with antibodies to target proteins, Baz1B (Abcam, ab50850), PSIP1 (Bethyl, A300-848A), DDX17 (Abcam, ab180190), PTPN6 (Santa Cruz, sc-287) or TSN (Sigma, HPA059561). As loading control membranes were reprobed with an antibody to beta-tubulin (Sigma, T6074). To screen for clones with disrupted *B2M*, single cell clones were stained with an antibody to MHC-I (eBioscience, HLA-ABC-FITC) and analyzed by flow cytometry.

Isolation and Culturing of Mouse $CD8^+$ T Cells

Naive $CD8^+$ OT-I cells were isolated from $Rag1^{-/-}$ OT-I transgenic mice. Lymph nodes and spleens were harvested and homogenized using the rubber end of a syringe and cell suspensions were filtered through a fine mesh. Cells were first enriched with anti-CD8 magnetic microbeads (CD8a, Ly-2 microbeads, mouse, Miltenyi Biotec) and then sorted on a FACSAria III Cell Sorter (BD Biosciences) to obtain cells with a $CD44^{lo}$ $CD62L^{hi}$ $CD8^+$ phenotype. OT-I cells ($CD90.1^+$) were cultured for 2 days in αCD3/αCD28 (2μg/ml) bound to NUNC 96 well MicroWell MaxiSorp plates (Sigma-Aldrich M9410) in the presence or absence of 3 mM L-arginine in the culture medium. On day 2 cells were transferred to U-bottom plates and cultured for 2 additional days in the presence of IL-2 (500 U/ml).

Adoptive T Cell Transfers and Survival Experiments

$CD90.1^+$ $CD45.1/2^+$ OT-I T cells were activated with plate-bound antibodies to CD3 and CD28 in control medium. OT-I cells with a different congenic marker ($CD90.1^+$ $CD45.1^+$) were activated in L-arginine-supplemented medium. At day 4, equal cell numbers were injected into the tail vein of $Cd3e^{-/-}$ host mice. To study the expansion of OT-I effector cells, host mice were sacrificed after 1, 3, 6, and 10 days post transfer and $CD90.1^+$ OT-I T cells from lymphoid organs (spleen and lymph nodes) were enriched with anti-CD90.1 microbeads (Miltenyi Biotec), stained and analyzed by FACS. The following monoclonal antibodies were used α-CD8α (53-6.7), α-CD44 (IM7), α-CD62L (MEL-14), α-CD90.1 (OX-7), α-CD90.2 (30-H12), α-CD45.1 (A20), α-CD45.2 (104).

Tumor Experiments: In Vitro Activation of T Cells

B16-OVA melanoma cells were cultured in RPMI 1640 plus 10% FCS, 1% penicillin/streptomycin and 2 mM glutamine. Before injection into mice, cells were trypsinized and washed twice in PBS. Then, $5x10^5$ cells were subcutaneously injected in the dorsal region of WT C57BL/6 mice. Ten days post injection, $5x10^6$ OT-I cells, that have been activated in vitro as described above, were injected into the tail vein of tumor-bearing mice. The size of tumors was measured in a blinded fashion using calipers.

Tumor Experiments: In Vivo Priming of T Cells

B16-OVA melanoma cells were cultured and injected into WT C57BL/6 mice as described above. Five days post injection, when tumors were very small, mice were γ-irradiated (5 Gy) and 24 hr later they received $4x10^5$ OT-I cells intravenously (i.v.). The day after mice were immunized intraperitoneally (i.p.) with SIINFEKL peptide ($OVA_{257-264}$) in Imject Alum Adjuvant (Thermo Fisher Scientific). L-Arg (1.5 g/Kg body weight) or PBS, as control, was daily orally administrated, starting one day before T cell transfer and until the end of the experiment. The size of tumors was measured in a blinded fashion using calipers.

Experiments with $Arg2^{-/-}$ Mouse T Cells

For in vitro experiments, $5x10^4$ FACS-sorted naive T cells were activated with plate-bound antibodies to CD3 (2 μg/ml) and CD28 (2 μg/ml). Two days after activation, T cells were transferred into U-bottom plates and IL-2 was added to culture media. Four days after activation, cells were washed extensively and plated in medium devoid of IL-2. Cell viability was measured two days after IL-2 withdrawal by Annexin V staining. For in vivo experiments, 10^6 FACS-sorted WT $CD8^+$ naive T cells ($CD45.1^+$) were transferred together with 10^6 FACS-sorted $Arg2^{-/-}$ $CD8^+$ naive T cells ($CD45.2^+$, $CD90.2^+$), into slightly γ-irradiated (3 Gy) WT mice ($CD45.2^+$, $CD90.1^+$). The day after, host mice were immunized subcutaneously (s.c.) with MHC class-I binding peptide SIINFEKL (Chicken Ovalbumin, OVA, amino acids 257-264, 15 μg/mouse) emulsified in Complete Freund's Adjuvant, CFA. CFA was prepared by adding

4 mg/ml of *M. tuberculosis* H37RA (Difco) to Incomplete Freund's Adjuvant, IFA (BD Biosciences). SIINFEKL peptide ($OVA_{257-264}$) was obtained from Servei de Proteòmica, Pompeu Fabra University, Barcelona, Spain. On day 15 post immunization, mice were euthanized and draining lymph nodes were collected and analyzed by flow cytometry. Cells were counted according to the expression of congenic markers and by gating on live $CD44^{hi}$, H-2Kb/$OVA_{257-264}$ $multimer^{+}$, $CD8^{+}$ cells. The H-2Kb/$OVA_{257-264}$ multimers were purchased from TCMetrix.

Mouse Experiments with Dietary L-Arginine

$2x10^5$ $CD90.1^{+}$ $CD4^{+}$ HA TCR-transgenic T cells, on a BALB/c background, were adoptively transferred in WT $CD90.2^{+}$ BALB/c mice. The day after, host mice were immunized s.c. with influenza $HA_{110-119}$ peptide (purchased from Anaspec) emulsified in CFA. L-Arg (1.5 g/kg body weight) or PBS, as control, was daily orally administrated, starting 1 day before T cell transfer and until the end of the experiment. Draining lymph nodes were analyzed on day 15 post immunization for the presence of transferred transgenic memory $CD44^{hi}$ $CD90.1^{+}$ $CD4^{+}$ T cells. Sera were collected 30 min after oral L-arginine administration to mice and L-arginine and L-threonine concentrations in sera were measured on a MassTrak (Waters) instrument at the functional genomics center in Zurich. To determine intracellular L-arginine levels, activated T cells were isolated from draining lymph nodes 60 hr after activation and 30 min after the daily L-arginine administration. Metabolites were extracted with hot 70% ethanol and analyzed by HILIC LC-MS/MS.

QUANTIFICATION AND STATISTICAL ANALYSIS

Statistical parameters including the exact value of n, the definition of center, dispersion and precision measures (mean ± SEM) and statistical significance are reported in the Figures and Figure Legends. Data were judged to be statistically significant when $p < 0.05$ by two-tailed Student's t test. In figures, asterisks denote statistical significance as calculated by Student's t test (*, $p < 0.05$; **, $p < 0.01$; ***, $p < 0.001$; ****, $p < 0.0001$). Survival significance in adoptive cell transfer studies was determined by a Log-rank test. Statistical analysis was performed in R or GraphPad PRISM 6.

Proteome Data

Data analysis was performed using the Perseus software and the R statistical computing environment. Missing values were imputed with a normal distribution of 30% in comparison to the SD of measured values and a 1.8 SD down-shift of the mean to simulate the distribution of low signal values (Hubner et al., 2010). Statistical significance between time points was evaluated by one-way ANOVA for each proteinGroup using a FDR of 0.1% and S_0 of 2 (S_0 sets a threshold for minimum fold change), unless otherwise noted (Tusher et al., 2001). For pairwise comparison, t test statistic was applied with a permutation based FDR of 5% and S_0 of 1.

Enrichment Analysis

Univariate test was performed on either all proteins or metabolites by t test with unequal variance (Welch Test). The resulting *P*-values were adjusted using the Benjamini-Hochberg procedure. Enrichment analysis was performed as suggested by Subramanian et al. (Subramanian et al., 2005). Both for metabolomics and proteomics data, we applied a permissive filtering with adj. p value less or equal than 0.1 and absolute log2(fold-change) larger or equal than 0.5. Enrichment *P*-values were calculated by the Fisher's exact test for all incremental subsets of filtered features ranked by the p value. For the 261 pathways defined by KEGG, the lowest *P*-value was retained as a reflection of the best possible enrichment given by the data independently of hard cut-offs. Eventually, enrichment *P*-values were corrected for multiple testing by the Benjamini-Hochberg method. In general, enrichments with an adjusted *P*-value < 0.05 were considered significant. Pathway enrichments were calculated independently for proteomics and metabolomics data. For metabolome-based enrichments, structural isomers in pathway were condensed and counted only once to account for the fact that the employed technology cannot distinguish between metabolite with identical molecular weight.

DATA AND SOFTWARE AVAILABILITY

The metabolomics and proteomics data are available in Tables S1 and S2. All software is freely or commercially available and is listed in the STAR Methods.

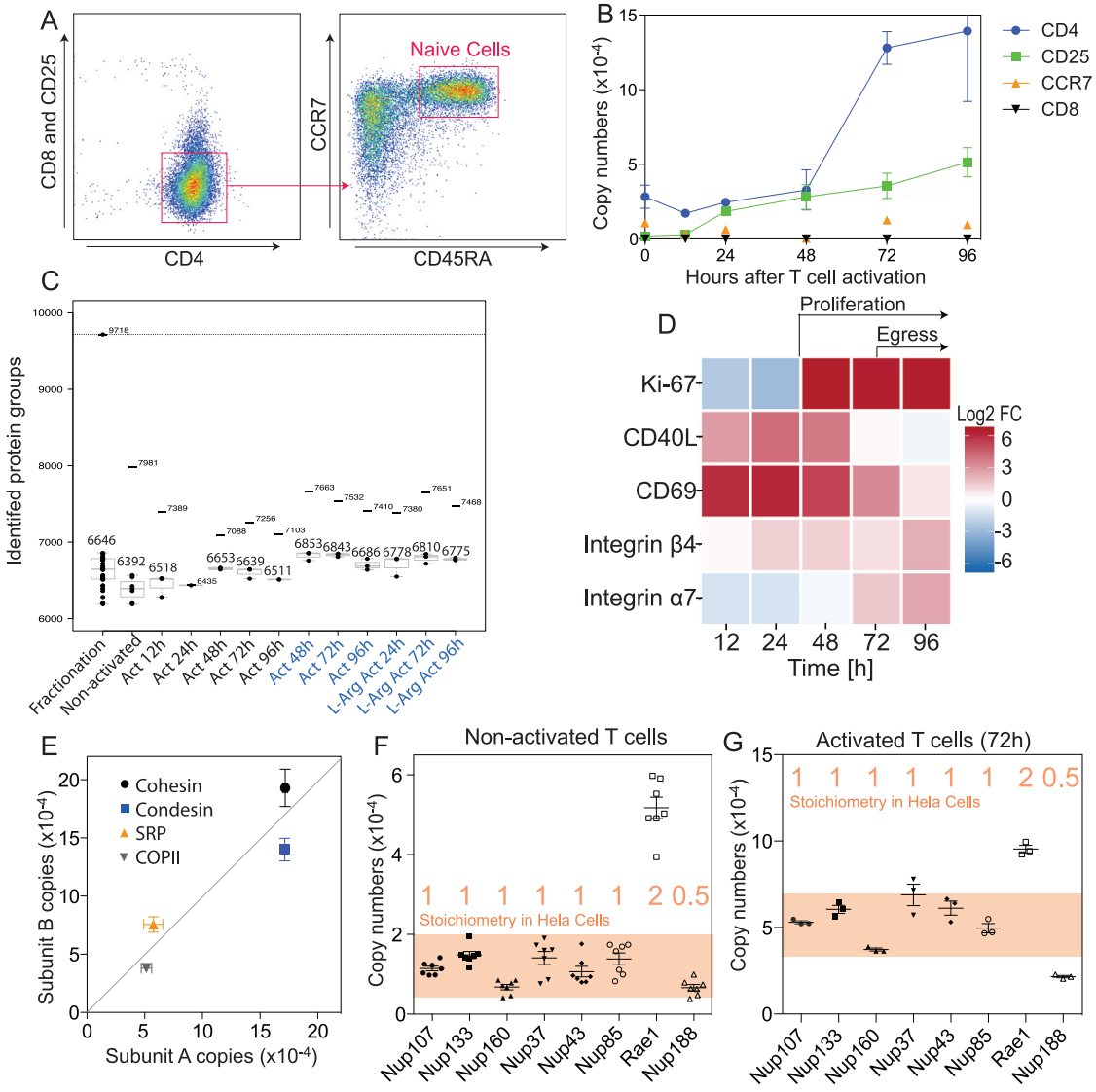

Figure S1. Quality Control of the Proteome Dataset, Related to Figure 1

(A) Sorting of human naive CD4$^+$ T cells. Shown are FACS plots of cells after enrichment with anti-CD4 magnetic beads. Cells were sorted as CD4$^+$ CCR7$^+$ CD45RA$^+$ and CD8$^-$CD25$^-$.

(B) Expression kinetics of indicated marker proteins. Bars represent the SEM of data from different donors, n = 7 (for resting cells), n = 3 (for 12h, 72h), n = 2 (for 96h, 48h), n = 1 (for 24h). CD25 and CD8 were not identified in resting cells. After activation, expression of CD25 increased whereas CD8 was never detected.

(C) Identified protein groups per condition. Taking all conditions together, a total of 9,718 proteins were identified. Per condition two numbers are indicated; the higher number indicates the total identifications and the lower number the mean of the single shots. Samples in blue were measured on a different instrument than samples in black. L-arg refers to 3 mM L-arginine.

(D) Relative protein abundance over time shown as a heat map. Log2 fold changes (FC) are relative to naive resting T cells. The marker for proliferating cells Ki-67 increased abruptly after 48h, when cells started to proliferate. CD40L expression increased immediately after activation and then decreased to initial levels. A similar expression pattern was observed for CD69, which inhibits egress from lymph nodes (Shiow et al., 2006). The expression of integrins α4 and β7 increased at later time points.

(E) Copy numbers of individual subunits of well-characterized protein complexes were plotted against each other. As the Sec23 subfamily includes Sec23A and Sec23B, their copy numbers were added up. The same was done for the subfamily members of Sec24 (A-D).

(F) Copy numbers of components of the nuclear pore complex (NPC). The stoichiometry of subunits measured using targeted quantitative proteomics (Ori et al., 2013) is indicated on the graph in red. Shown are copy numbers measured in naive resting T cells from seven donors.

(G) Same as in (F) but shown are copy numbers measured from activated cells (72h). n = 3 from three donors. Note that the numbers of Nup107 increased from 11,464 ± 1620 to 53,091 ± 1471. (A and E–G) Error bars represent SEM throughout.

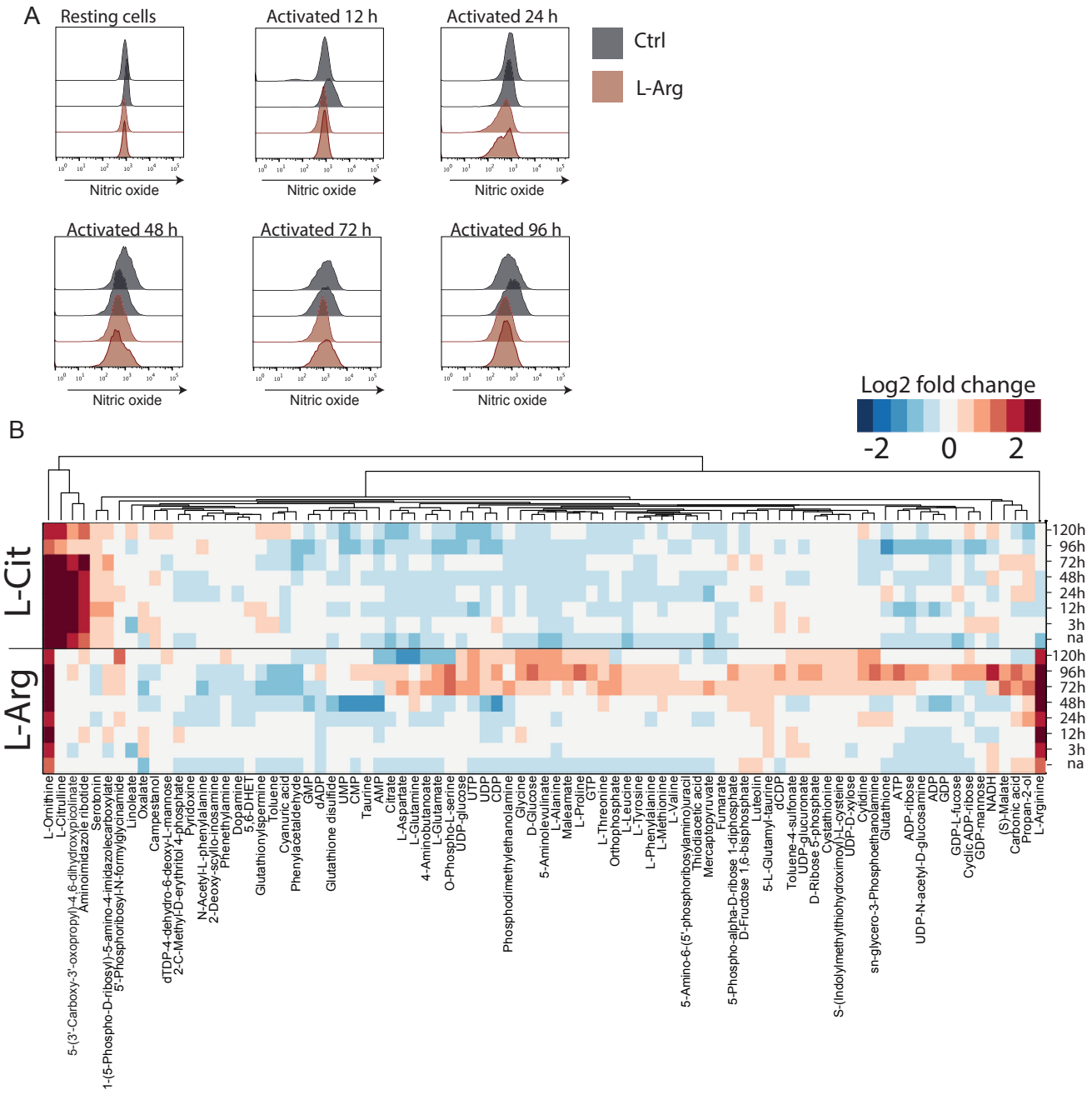

Figure S2. Impact of L-citrulline on Metabolism, Related to Figure 3

(A) Human naive CD4$^+$ T cells were activated in normal medium or in L-Arg medium. Nitric oxide formation was measured using DAF-FM diacetate at different time points.

(B) T cells were activated in control medium (Ctrl, containing 1mM L-arginine), or in medium supplemented with 3mM L-arginine (L-Arg) or 3mM L-citrulline (L-Cit) and harvested at different time points. The heat map shows the difference in the abundance of metabolites in T cells cultured in L-Arg- or L-Cit-medium compared to controls. Shown are only metabolites with a log2 fold change > 1 and an adjusted p value of < 0.05. n = 6 from one donor.

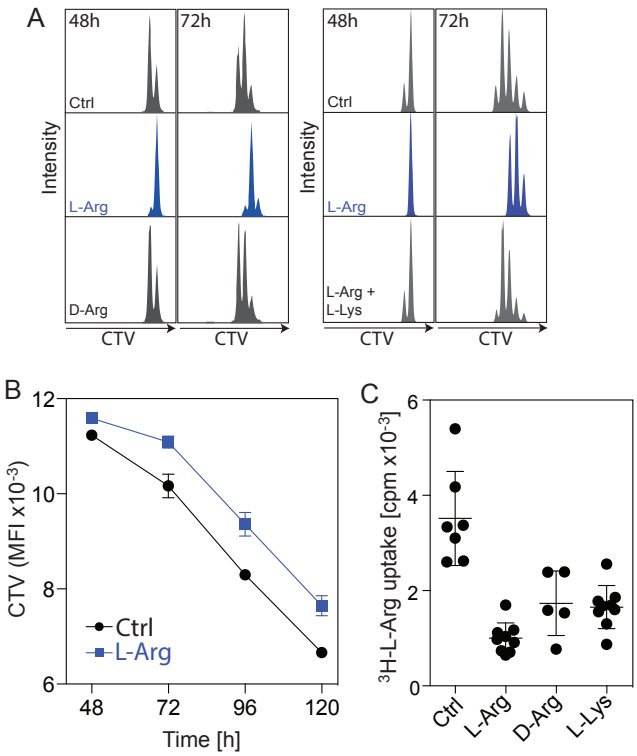

Figure S3. L-Arginine Delays the Onset of Proliferation, Related to Figure 4

(A) Kinetics of T cell proliferation. Human naive $CD4^+$ T cells were labeled with CellTraceViolet (CTV) and activated in Ctrl medium or in L-Arg medium or in medium supplemented with 3 mM D-arginine or 3 mM L-arginine together with 3 mM L-lysine. Cell divisions were monitored at 48h and 72h by flow cytometry.

(B) CTV-labeled $CD4^+$ T cells were activated in normal medium or L-Arg medium and the dilution of CTV was measured over time by flow cytometry. n = 5 from two donors.

(C) ^{3}H-L-arginine uptake by 3 day-activated $CD4^+$ T cells during a 15 min pulse. Where indicated, 3 mM L-arginine, D-arginine or L-lysine was added to the culture medium as a competitive uptake inhibitor. n = 7 for control, n = 9 for L-Arg, n = 5 for D-Arg, and n = 9 for L-Lys. Error bars represent SEM throughout.

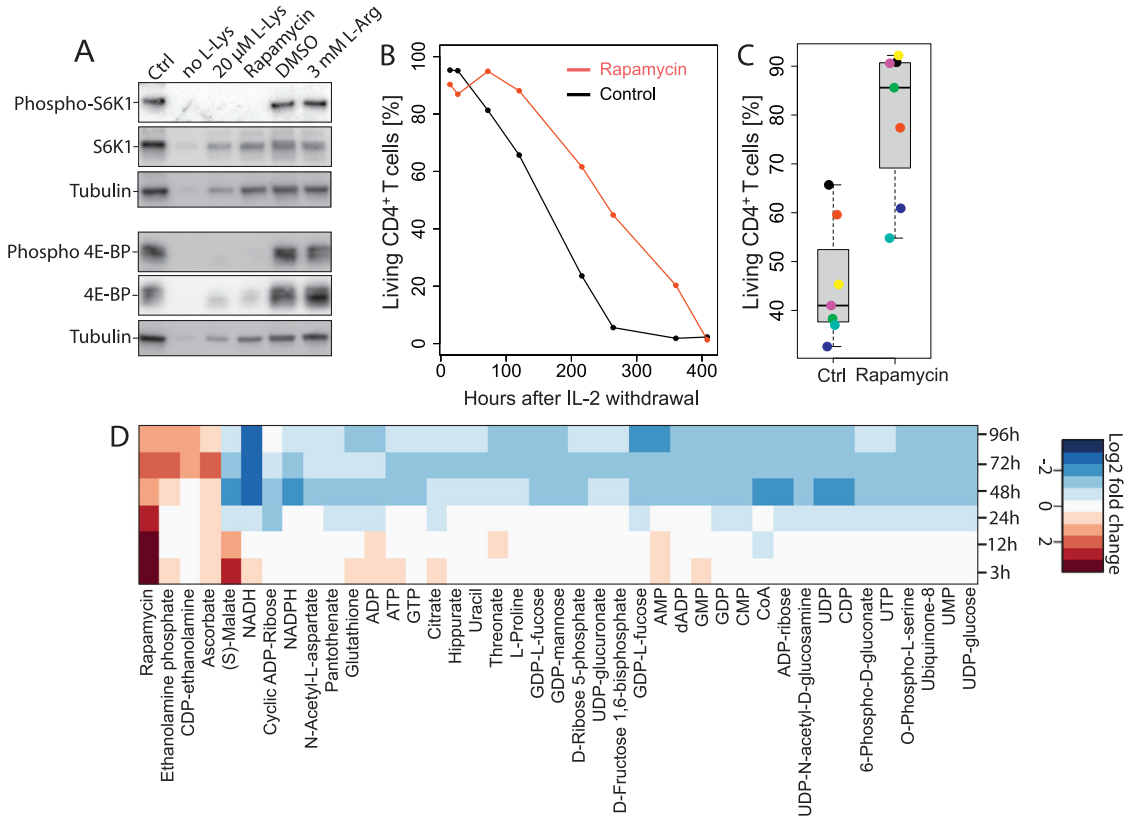

Figure S4. L-Arginine Increases the Survival of Activated T Cells Independent of mTOR Signaling, Related to Figure 4

(A) Human naive CD4$^+$ T cells were activated for 4 days, lysed and the phosphorylation levels of S6K1 (pThr389) and 4E-BP (pThr37/46) were analyzed by western blot. Rapamycin inhibited the phosphorylation of the mTOR targets, while DMSO or supplementation of the culture medium with 3 mM L-arginine had no effect. T cells hardly proliferated upon activation in culture medium containing no or 20 μM L-lysine and therefore phosphorylation of the target proteins could not be assessed.

(B) T cell survival experiment. Human naive CD4$^+$ T cells were activated in Ctrl medium or in medium containing 100 nM rapamycin. On day 5, cells were washed to withdraw IL-2 and cell survival was measured at different time points.

(C) Same as in (B) but cell survival was only measured 5 days after IL-2 withdrawal. n = 7 from seven donors. Boxplot. Same as in Figures 2A and 2B.

(D) Metabolic profiling of CD4$^+$ T cells activated in medium containing 100 nM rapamycin. The heat map shows the difference of metabolite abundances between rapamycin-treated cells and controls. n = 10 from two donors.

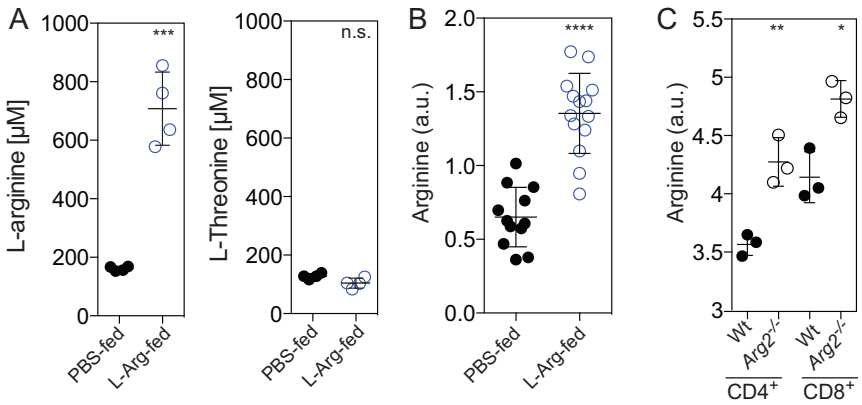

Figure S5. Oral Administration of L-Arginine Increases L-Arginine Levels in Mouse Sera and T Cells, Related to Figure 5

(A) BALB/c mice were administered L-arginine (1.5 mg/g body weight) and sera were collected after 30 min. L-arginine and, as a control, L-threonine concentrations were analyzed on a MassTrak amino acid analyzer. n = 4.

(B) BALB/c mice were immunized with ovalbumin in CFA. Sixty hours later, activated T cells from draining lymph nodes were enriched using magnetic beads coated with antibodies to CD44. Metabolites were extracted using hot 70% ethanol and L-arginine and L-glutamine levels (as an internal standard) were measured using LC-MS/MS. Shown is the ratio between L-arginine and L-glutamine intensities. n = 14.

(C) Intracellular L-arginine levels of wild-type and *Arg2*$^{-/-}$ CD4^{+} and CD8^{+} T cells 4 days after activation. n = 3. For statistical tests, a two-tailed unpaired Student's t test was used throughout, n.s. non significant; *$p < 0.05$; **$p < 0.005$; ***$p < 0.0005$; ****$p < 0.0001$. Error bars represent SEM throughout.

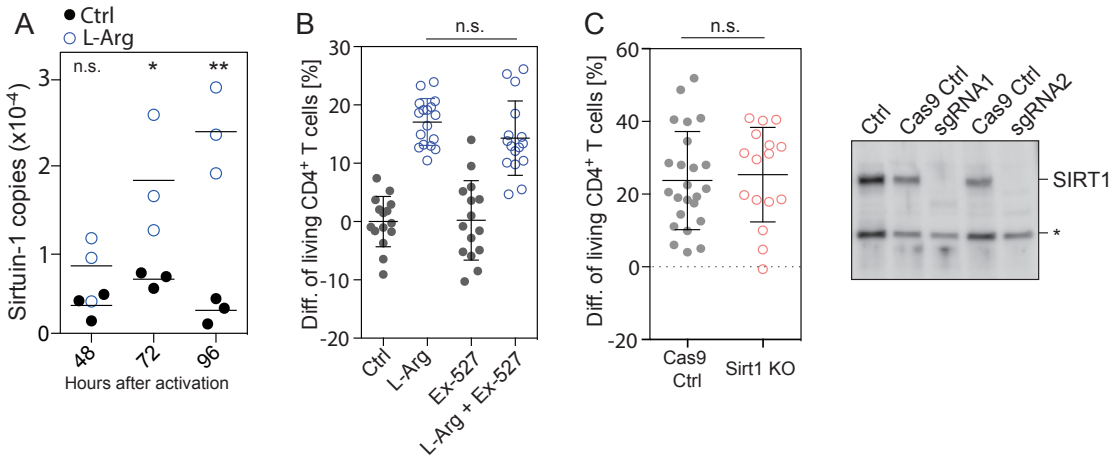

Figure S6. L-arginine Upregulates Sirtuin-1, Related to Figure 6

(A) Copy numbers of Sirtuin-1 (SIRT1) as determined by quantitative MS in human naive $CD4^+$ T cells activated in normal medium or L-Arg-medium. n = 3 from three donors.

(B) T cell survival experiment. The Sirtuin-1 inhibitor Ex-527 was added at the time point of activation at a concentration of 5 μM. n = 16 from four donors.

(C) T cell survival experiments with clones expressing Cas9 only, or clones devoid of Sirtuin-1. n = 16 from 6 clones. Right panel: western blot of two different Sirtuin-1 knockout clones generated with different sgRNAs. * unspecific band. For statistical tests, a two-tailed unpaired Student's t test was used throughout, n.s. non significant; *$p < 0.05$; **$p < 0.005$; ***$p < 0.0005$; ****$p < 0.0001$. (B and C) Error bars represent SEM throughout.